CNRS
Centre National de la Recherche Scientifique

INFN
Istituto Nazionale di Fisica Nucleare

Simulations of Advanced Virgo recycling cavities and thermal effects Part 2

VIR-0167A-10

Gabriele Vajente[1], Julien Marque[2]
[1] *INFN sezione di Pisa and Pisa University*
[2] *European Gravitational Observatory*

Issue: 1
Date: March 4, 2010

VIRGO * A joint CNRS-INFN Project
Via E. Amaldi, I-56021 S. Stefano a Macerata - Cascina (Pisa)
Secretariat: Telephone (39) 050 752 521 * FAX (39) 050 752 550 * Email W3@virgo.infn.it

Contents

1 Introduction

This notes is an integration of the results previously described in [1]. For completeness with respect to the previous note the response of NDRC to differential mis-alignment is briefly studied. The behavior of SRC control sidebands (56 MHz) is described here, first in the broad-band (zero detuning) case and then in the detuned configuration which is the baseline one [3]. Simulation of arm cavity mirrors of finite size is also presented here.

A new algorithm can be used to optimize the working point by zeroing the simulated error signals. The algorithm and results for NDRC are discussed.

2 Non-degenerate Recycling Cavities and differential mis-alignments

Fig. 1 shows that a small differential mis-alignment of the two cavity input mirrors (± 25 nrad) can have a significant effect on the fundamental mode 6 MHz sidebands when the SRC crosses a tuning that makes the first transverse mode resonant inside SRC. The reduction of recycling gain might seem small, but the largest effect concerns the sidebands phase. Indeed when a HOM resonance is crossed, one of the two sideband is unperturbed, while the other one sees a spurious dephasing that can be as large as few degrees. This dephasing can be disastrous if the sideband is used for example for frequency stabilization, since it is equivalent to few spectral ranges of the arm cavities.

The simulation proves that the differential weakness of NDRC exists for all high order modes.

As already pointed out in [1] this differential weakness might not be a issue in the steady state configuration, since a proper optical design could be able to move the resonance points of high order modes (up to a reasonable order) far enough from the desired final tuning. However differential problems pose very stringent requirements on the lock acquisition procedure: if during SRC acquisition the tuning crosses the resonant point of one high order mode in presence of small mis-alignments or residual lensings the interferometer control is likely lost because of the loss or dephasing of one of the two sidebands. This means that it must be ensured that signal recycling mirror never crosses these points, even during the first stages of lock acquisition. This seems unfeasible in practical experiments.

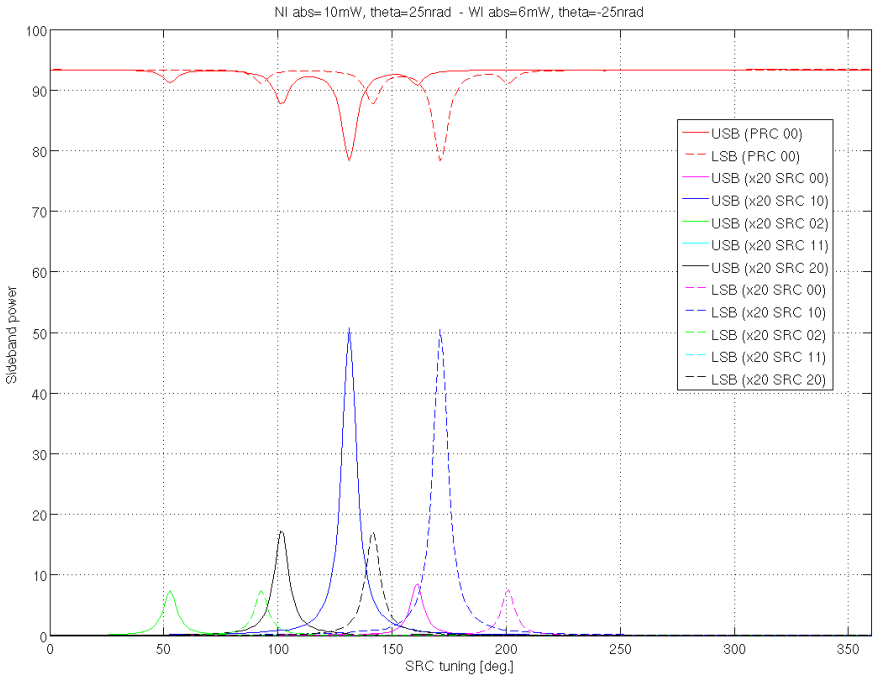

Figure 1: Scan of the signal recycling cavity tuning to show the effect of high order mode resonance inside SRC. The two input mirror are differentially mis-aligned by 25 nrad and small thermal lensings have been added.

3 Second sideband behavior

3.1 SRCL control

An error signal to control SRCL must be extracted from the second modulation frequency, which is the only one to be significantly transmitted inside the SRC. In the case of zero detuning of the signal recycling cavity (broad-band operation) the carrier is anti-resonant inside SRC and it is therefore possible to choose a macroscopic length of SRC to have both upper and lower second sidebands simultaneously resonant inside SRC. The line-width of SRC as seen by the second sidebands depends on the SR mirror reflectivity and on the value of Schnupp asymmetry.

In the case of detuned signal recycling, it is no more possible to have both sidebands simultaneously resonant at the detuned position. There are two possible choices for the macroscopic SRC length: it can be tuned to have one of the two sidebands at resonance for the desired detuning and the other not resonant; or it can be left at the optimal position to have both sidebands resonant for the broad-band condition. See fig. 2 for reference. In the first case the error signal can be extracted from a power recycling cavity pick-off and it crosses zero only when SRC detuning is zero. The plot shown in fig. 2 refers to a Schnupp asymmetry of 3 cm, which is too small to use the error signal inside its linear range with 0.15 rad detuning. However if the Schnupp asymmetry is increased to 10 cm (see fig. 3) the linear range of this signal extends up to about 0.3 rad.

If the macroscopic length is chosen to have only one sideband resonant at 0.15 rad detuning, the error signal shows multiple zeros with different signs: the single one still at zero, the double one at a detuning which depends on the choice of demodulation phase. It is possible to choose it to have th error signal crossing zero at the desired detuning. However the linear range is small and it is not possible to have a smooth transition from 0 to 0.15 rad detuning.

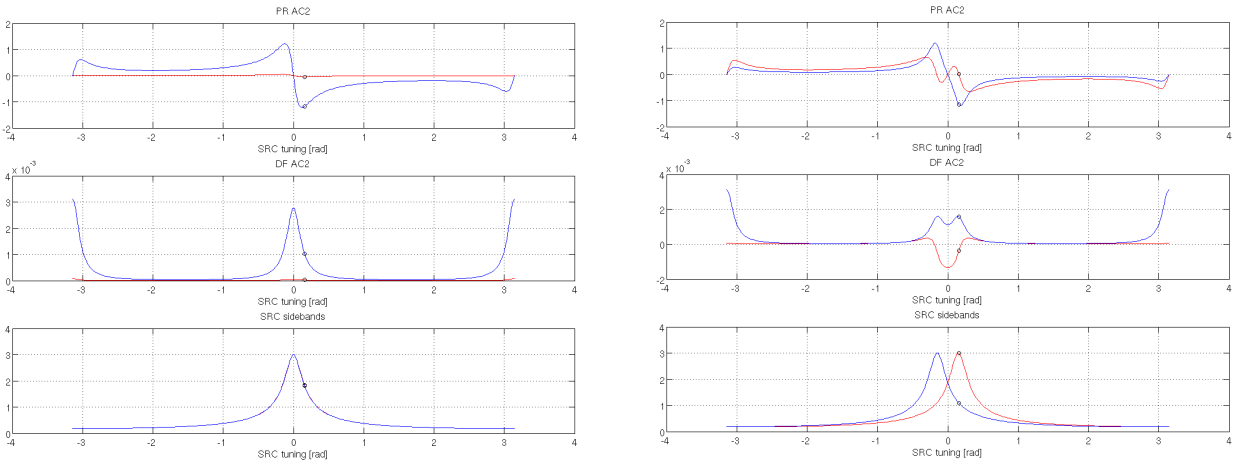

Figure 2: Comparison of possible signal recycling error signals for a SRC macroscopic length tuned to have both sidebands resonant for broad-band configuration (left) and to have one sideband resonant for 0.15 rad detuning (right). The circles shows the 0.15 rad detuned position.

For these reasons we choose to tune the signal recycling cavity macroscopic length in order to have both sidebands resonant in the broad-band configuration and to increase the Schnupp asymmetry to 10 cm to enlarge the linear range of the SRC error signal.

All the following results are obtained with simulations performed as explained in [1]: they show the behavior of 56 MHz sidebands as a function of the thermal lensings in the two input mirrors. For both NDRC and MSRC first the broad-band configuration is studied to gain some insight on the sideband behavior: in this case SRC is not locked and maintained at the nominal zero tuning. Then the detuned case is considered.

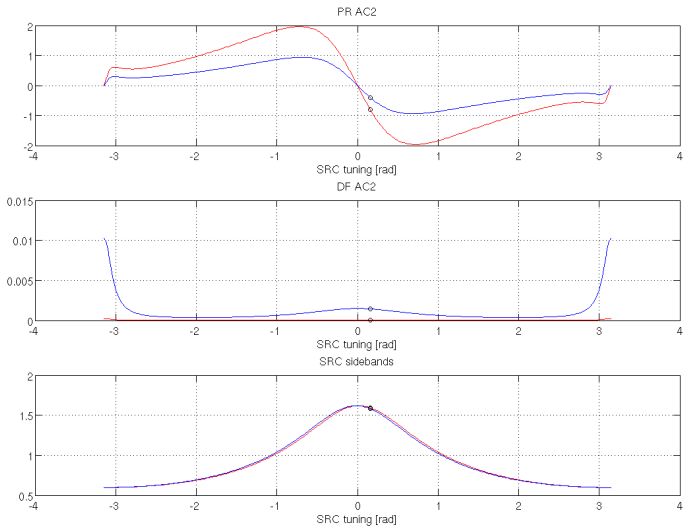

Figure 3: Possible signal recycling error signals for 10 cm Schnupp asymmetry and macroscopic length tuned for broad-band.

3.2 Marginally stable recycling cavities - Broad-band

Figures 4 and 5 show the second sideband powers inside the power recycling cavity as a function of thermal lensings, when the SRC tuning is zero. In this condition both sidebands are resonant inside SRC. The two sidebands appears balanced inside PRC at zero lensing, with a recycling gain of about 25, which is the one expected from the PR reflectivity and Schnupp asymmetry when the SRC is on resonance. When some lensing is added, the two sidebands becomes unbalanced: indeed the two recycling gains are maximum at two lines parallel to the main diagonal. In presence of differential lensings, the upper sideband reflected from the north arm acquires an additional dephasing opposite to the one reflected from the west arm. There exists a differential lensing that makes this phase cancels the dephasing coming from the Schnupp asymmetry: at all these points the upper sideband is not transmitted inside SRC and therefore its PRC recycling gain is not depressed by the SRC resonance. Clearly the differential lensing that cancel the Schnupp asymmetry for the lower sideband is the opposite one with respect to the upper. Finally, superimposed with the differential effect, there is the well known degeneration effect due to common mode, which depress the recycling gain for increasing lensing. Since the power recycling cavity finesse is lower for the 56 MHz sidebands than for the 6 MHz one, the common lensing reduction of gain is slightly smaller for 56 MHz sidebands than for 6 MHz one.

Figures 6 and 7 show the second sideband powers inside the signal recycling cavity. These plots are complementary to those in fig. 4 and 5. Indeed when the power recycling gain is high there is almost no sideband transmitted to SRC. This happens on the two off-diagonal lines which depends on the Schnupp asymmetry. These figures refers to a 3 cm Schnupp asymmetry. If it is increased to 10 cm as discussed in sec. 3.1, the critical lines move far away from the central part of the map and the problem can be neglected as will be shown in the next section.

3.3 Marginally stable recycling cavities - detuned

Figures 8 and 9 show the 56 MHz sideband powers inside PRC with a detuned signal recycling cavity. They are to be compared with figures 4 and 5. At null thermal lensing the recycling gain for these sidebands is larger due to the fact the SRC is out of resonance for both of them. At the level where the Schnupp asymmetry is canceled by differential effects one gets the same gain as in the tuned cases. This is expected since the SRC plays no role if the effective Schnupp asymmetry is null.

Figures 10 and 11 show the sideband powers inside signal recycling cavity. The power is lower here with respect to the broad-band case, since as already explained the sidebands are no more resonant inside SRC. The map shows two region of larger power, which corresponds to small or large differential lensing: in the second region the dephasing introduced by the differential thermal effects is large enough to reverse the Schnupp asymmetry.

Finally figures 12, 13, 14 and 15 show the same analysis with Schnupp asymmetry increased to 10 cm. As already explained, the region of small transmission of 56 MHz sidebands to SRC is moved away from the central part of the plots, thus becoming no more really relevant. Moreover, the cold state powers inside PRC are smaller than in the 3 cm case, while the powers inside SRC are larger.

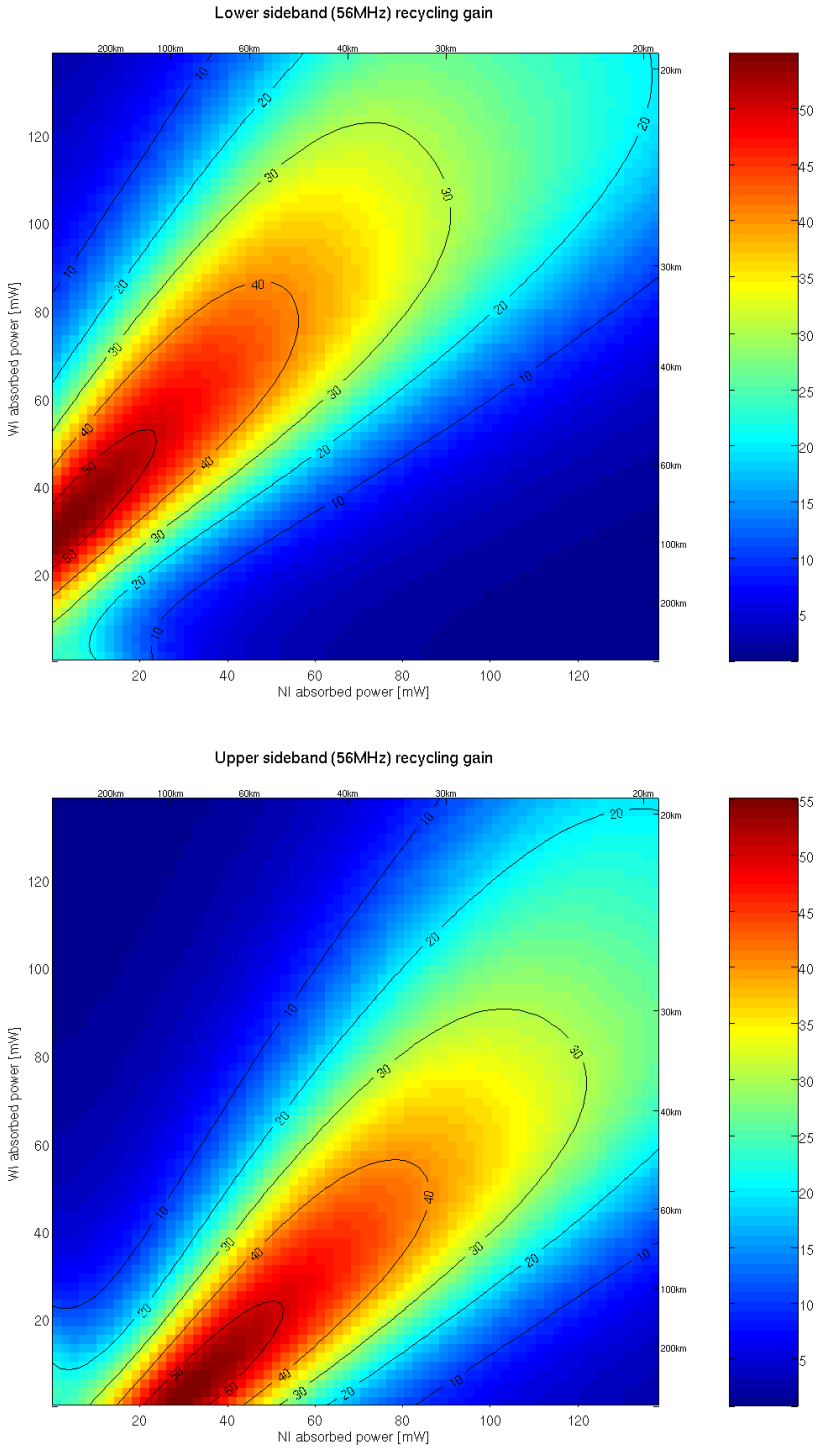

Figure 4: **MSRC Schnupp 3 cm broadband** Power inside PRC for the 56 MHz sidebands (all modes).

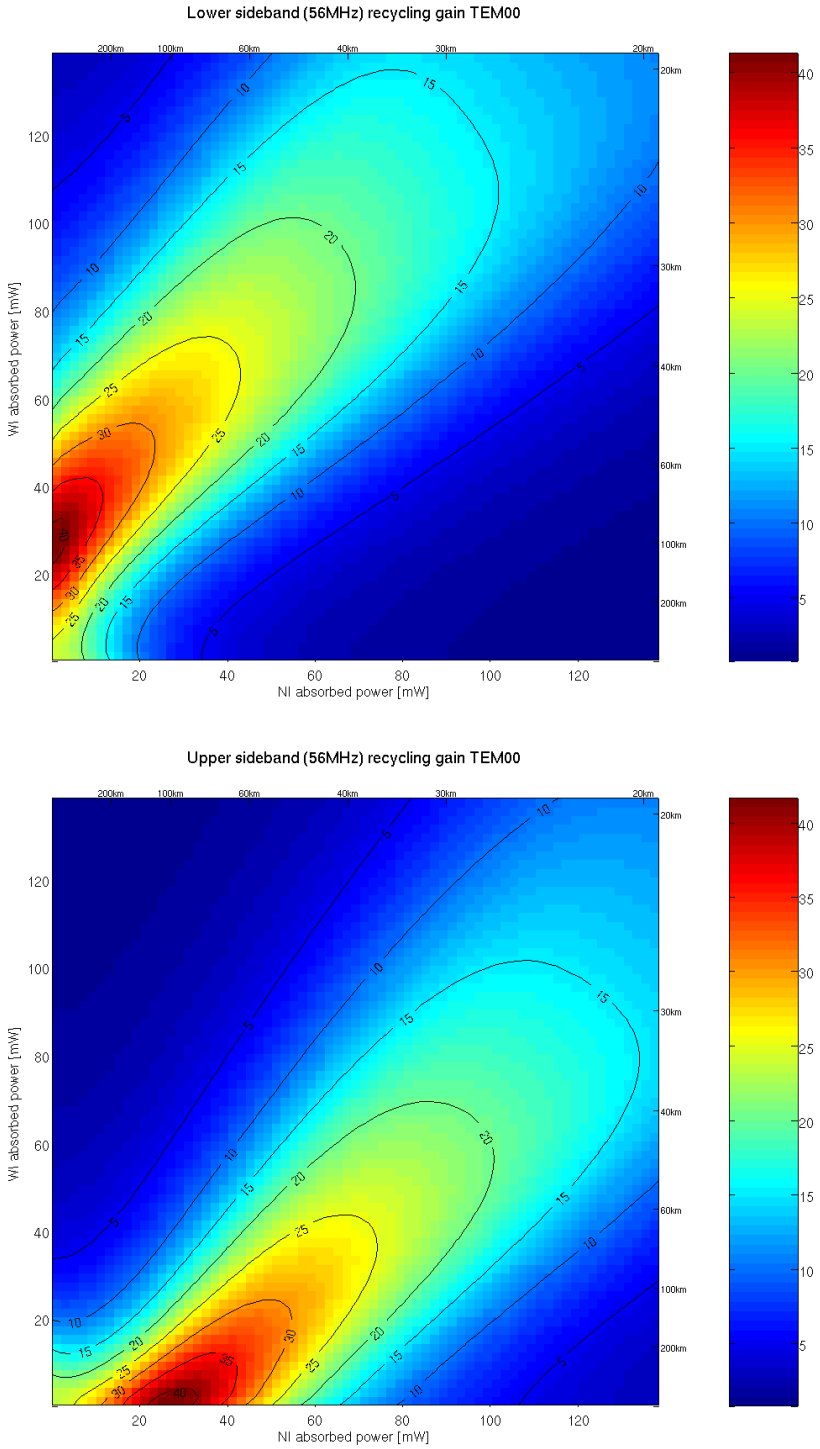

Figure 5: **MSRC Schnupp 3 cm broadband** Power inside PRC for the 56 MHz sidebands (only TEM_{00}).

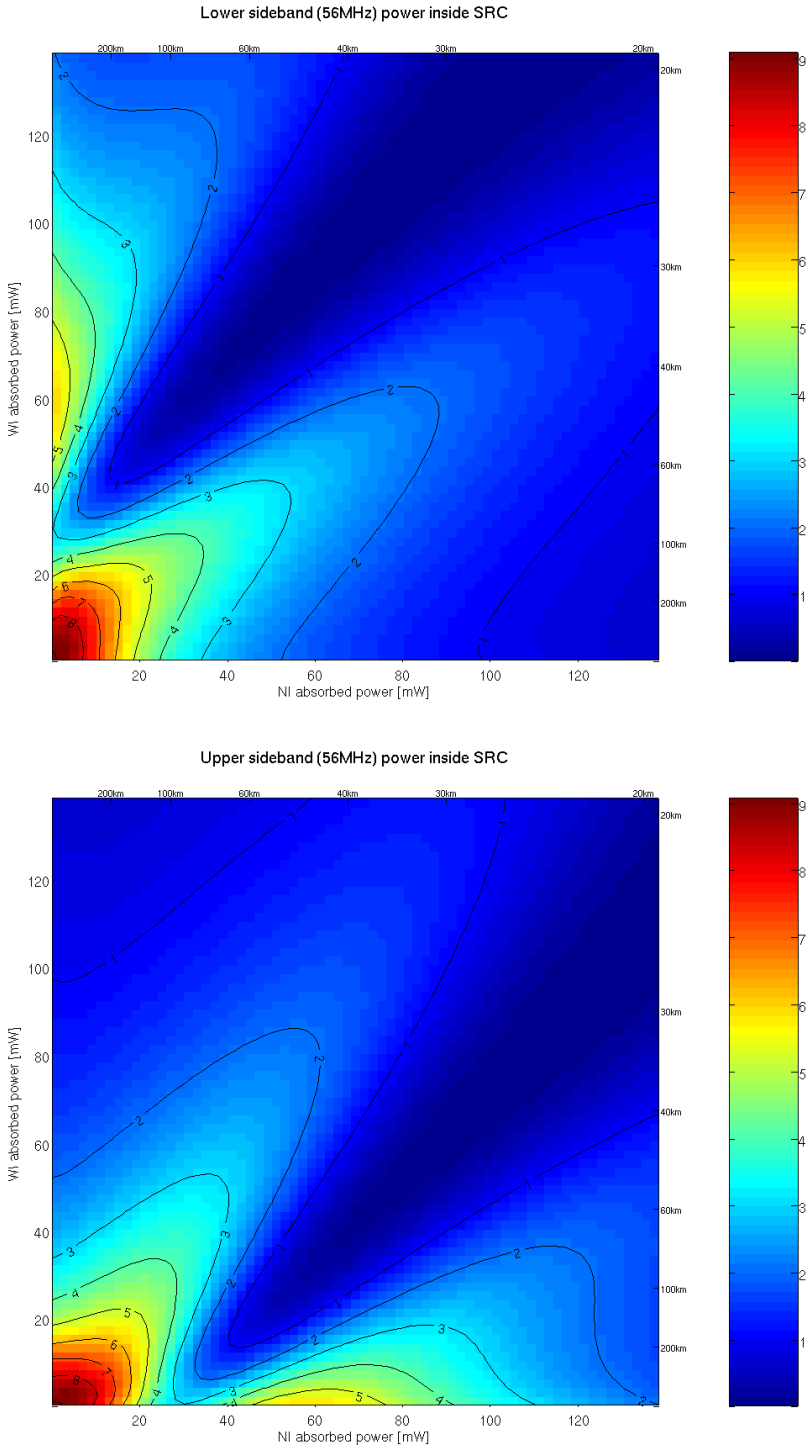

Figure 6: **MSRC Schnupp 3 cm broadband** Power inside SRC for the 56 MHz sidebands (all modes).

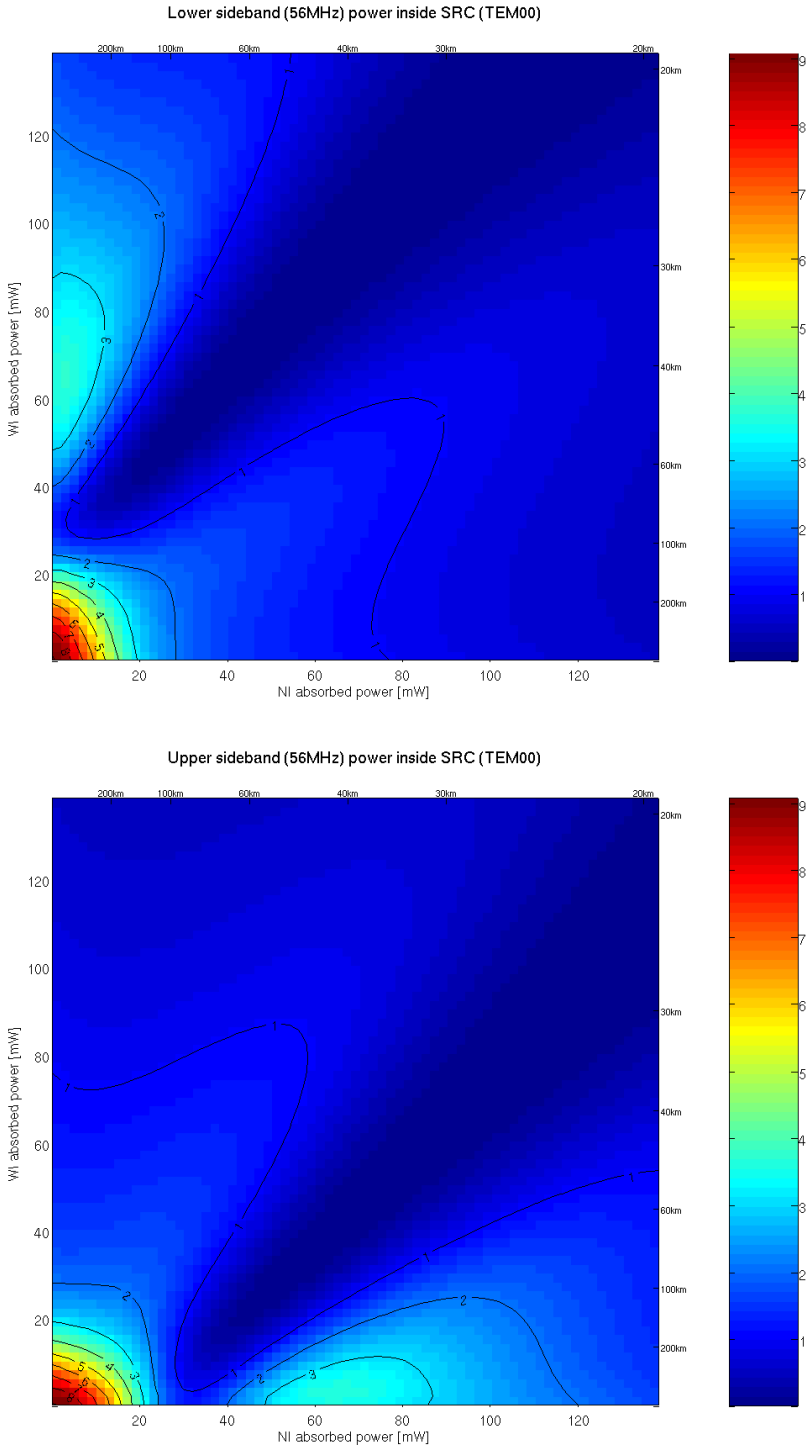

Figure 7: **MSRC Schnupp 3 cm broadband** Power inside SRC for the 56 MHz sidebands (only TEM_{00}).

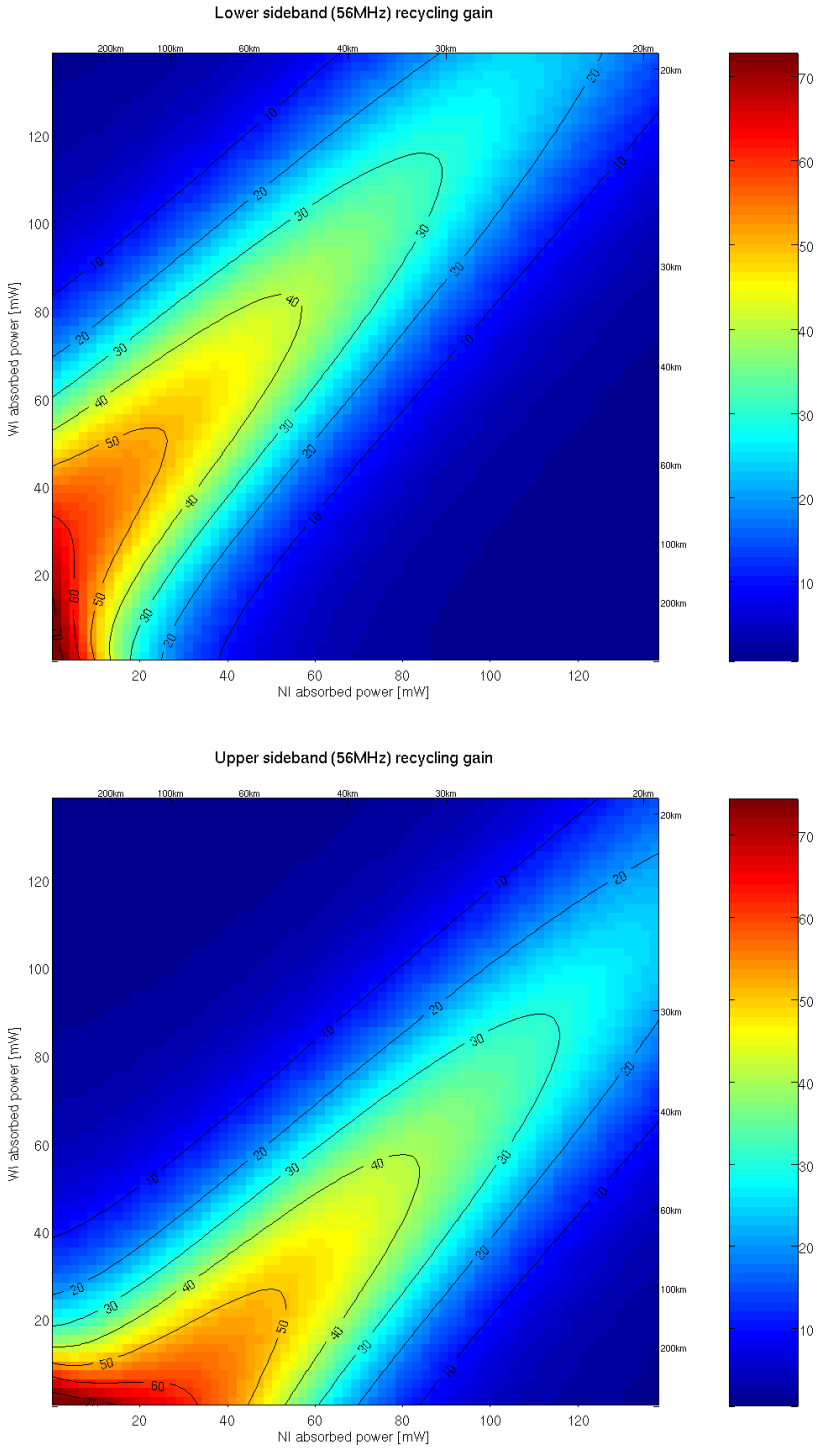

Figure 8: **MSRC Schnupp 3 cm detuned** Power inside PRC for the 56 MHz sidebands (all modes).

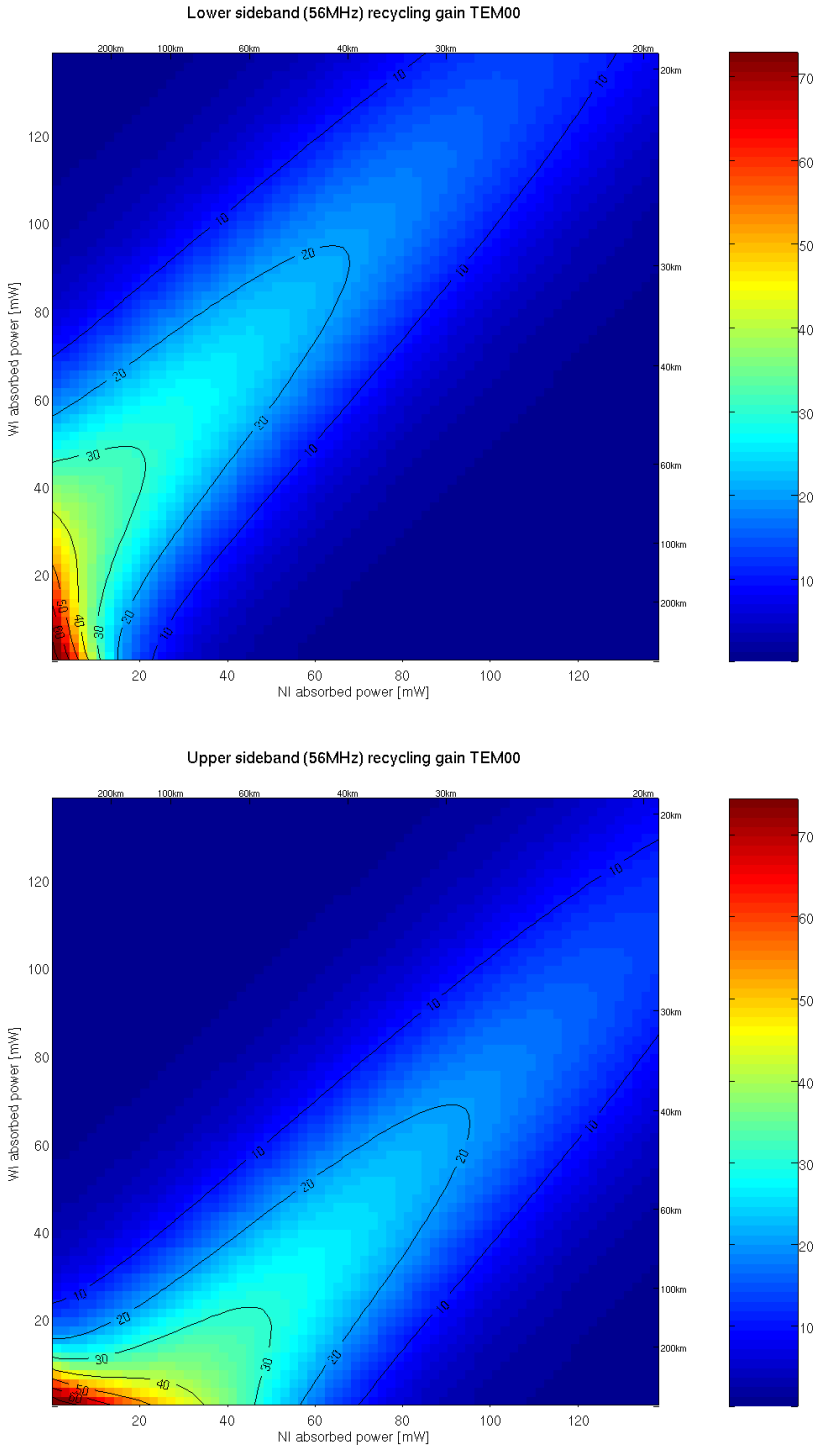

Figure 9: **MSRC Schnupp 3 cm detuned** Power inside PRC for the 56 MHz sidebands (only TEM_{00}).

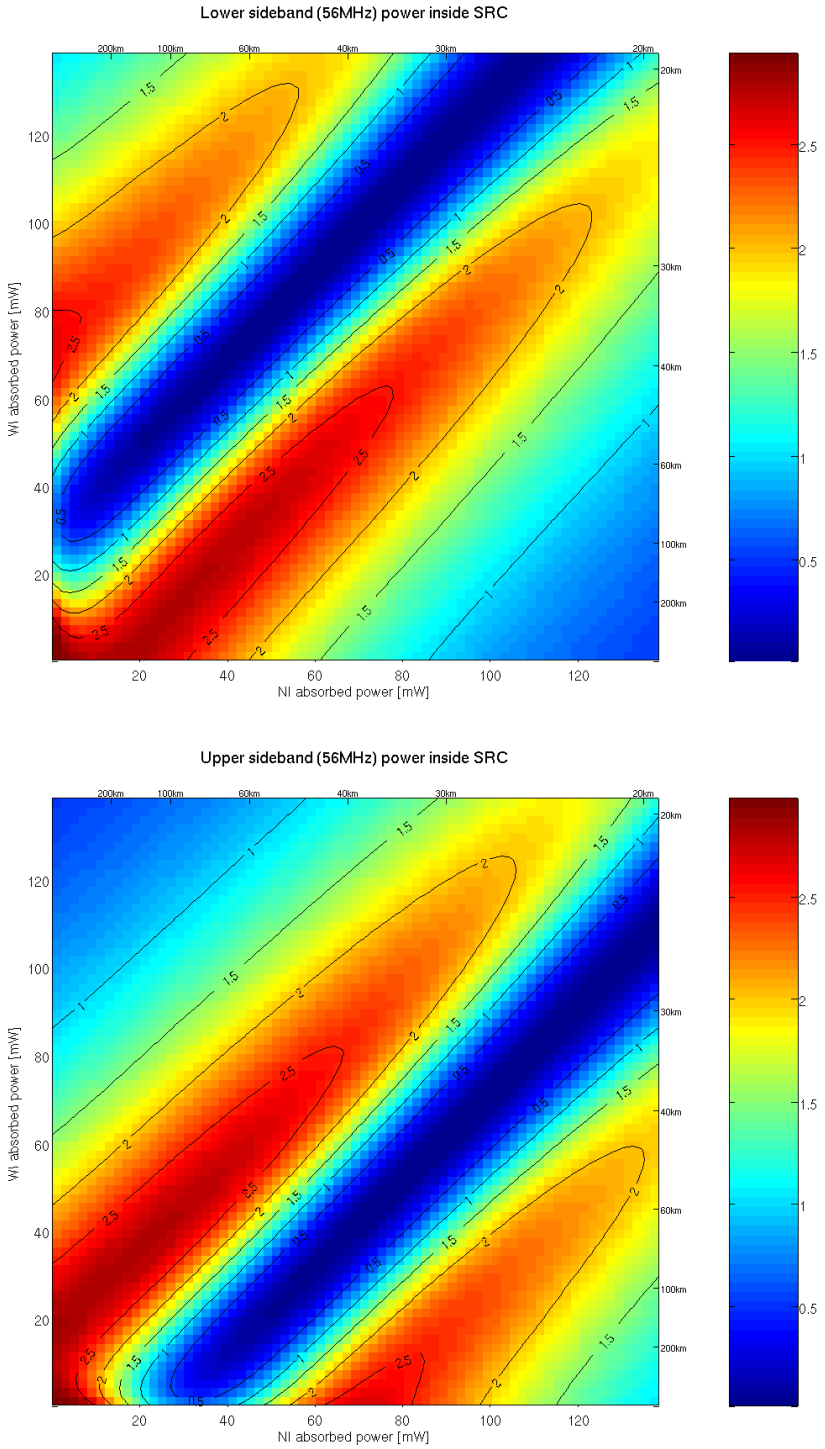

Figure 10: **MSRC Schnupp 3 cm detuned** Power inside SRC for the 56 MHz sidebands (all modes).

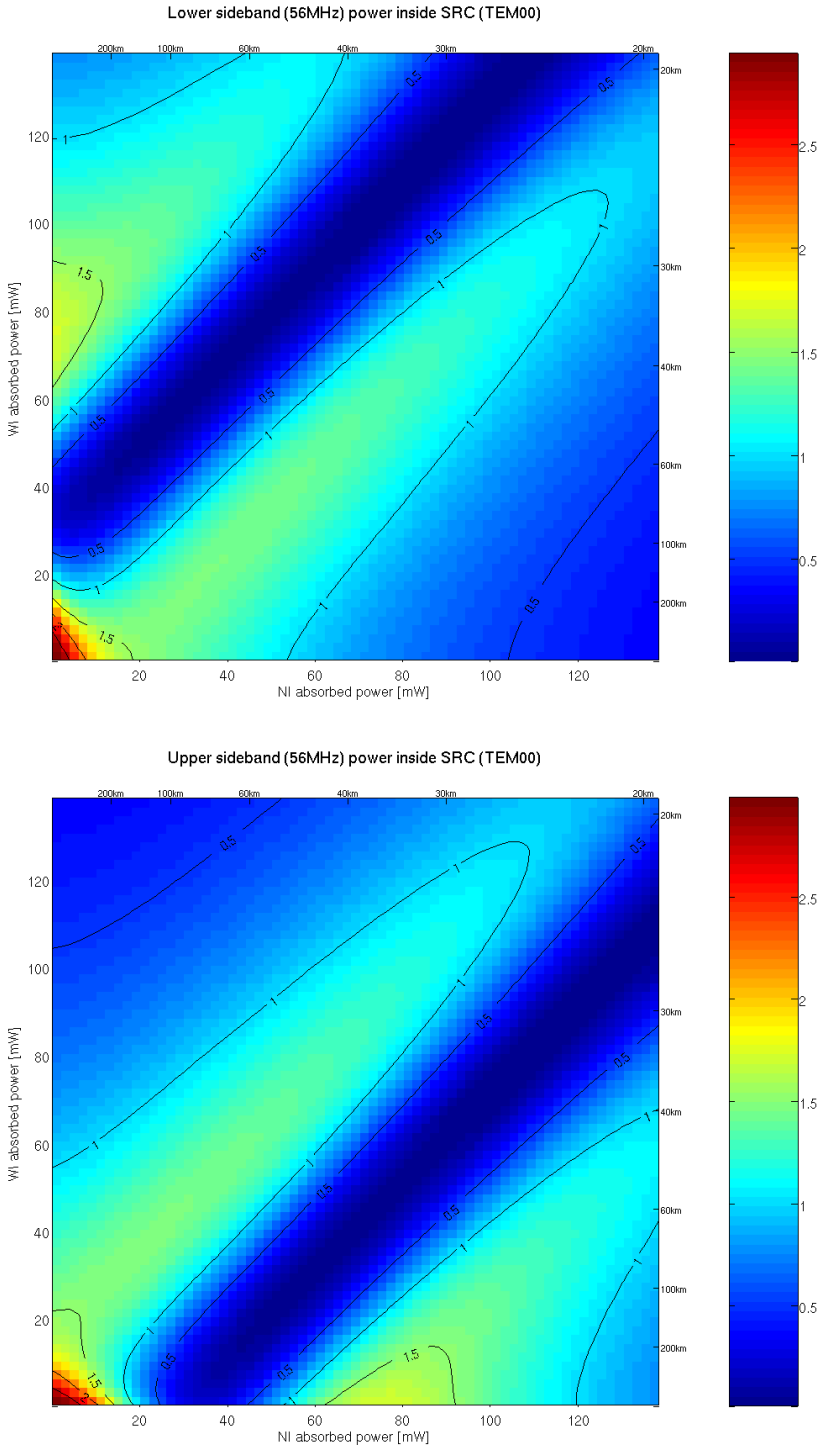

Figure 11: **MSRC Schnupp 3 cm** Power inside SRC for the 56 MHz sidebands (only TEM_{00}).

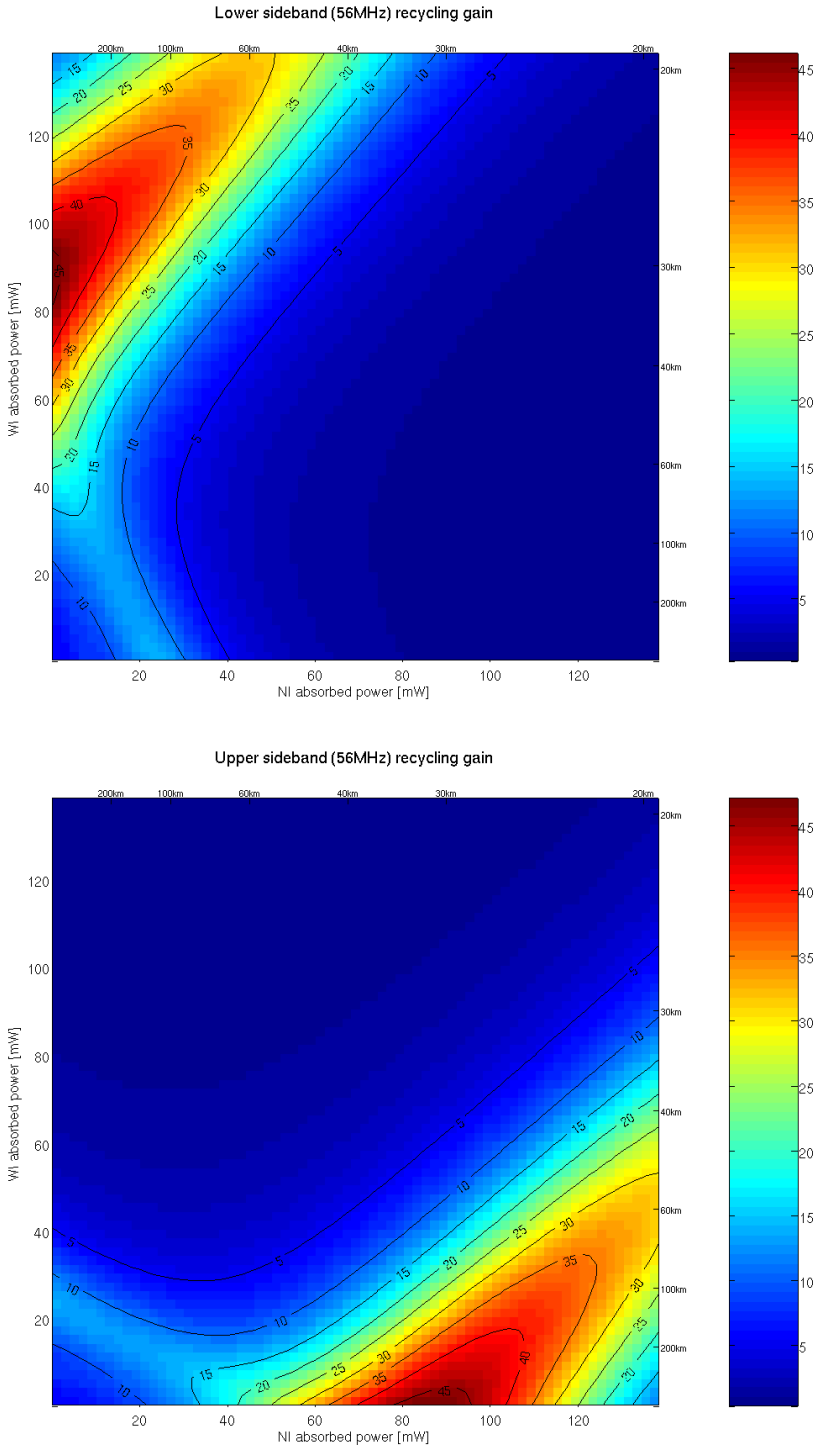

Figure 12: **MSRC Schnupp 10 cm detuned** Power inside PRC for the 56 MHz sidebands (all modes).

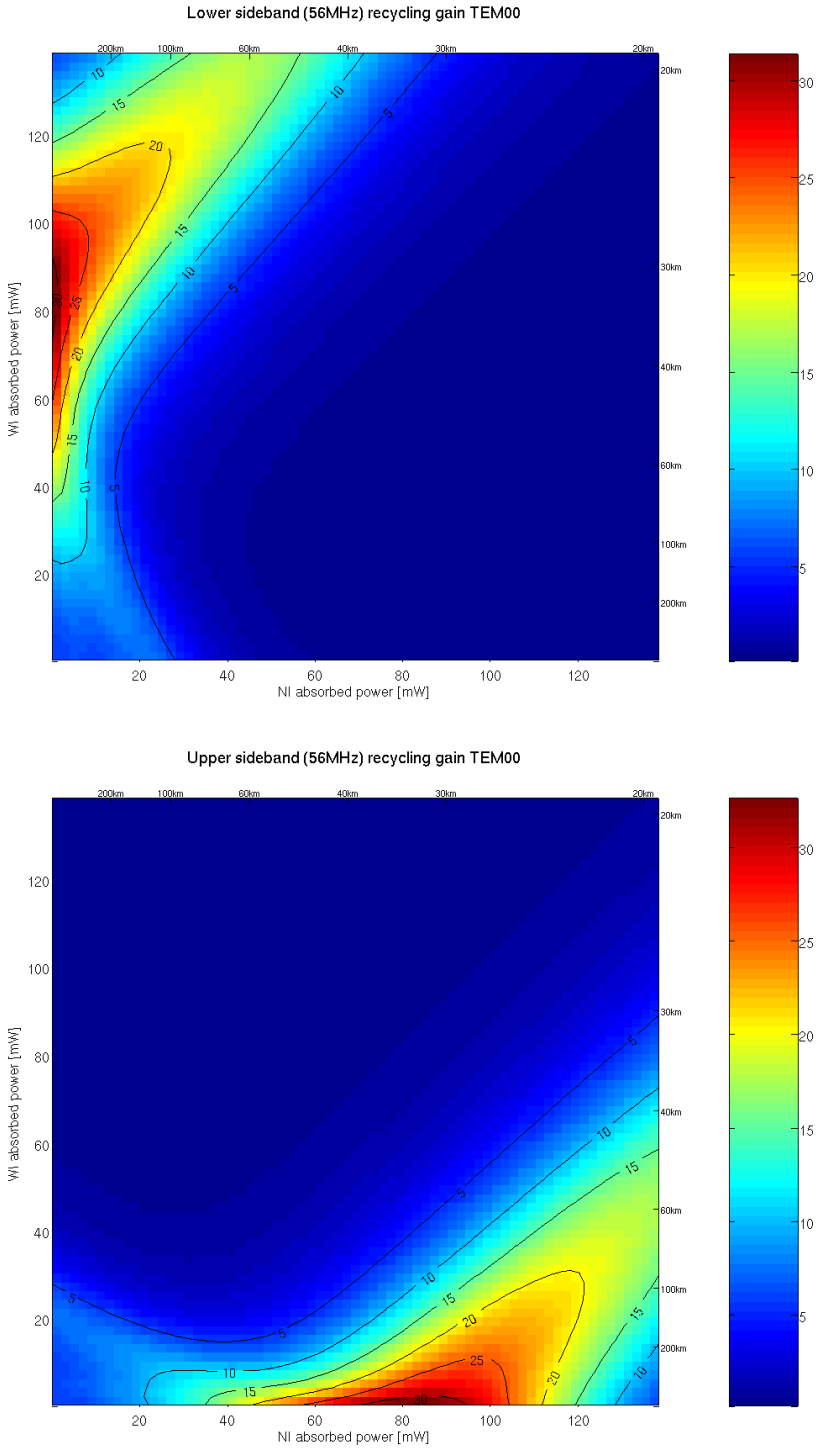

Figure 13: **MSRC Schnupp 10 cm detuned** Power inside PRC for the 56 MHz sidebands (only TEM_{00}).

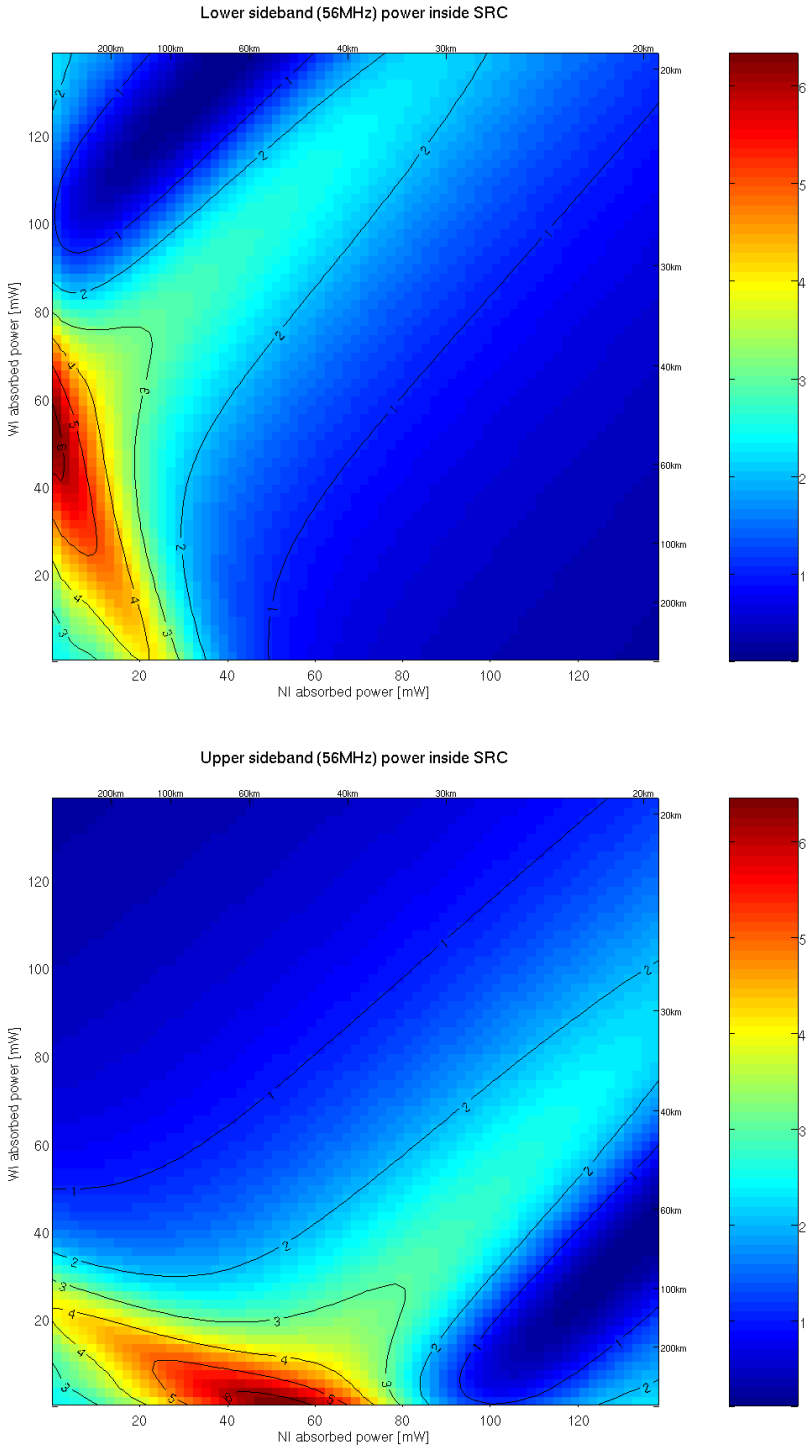

Figure 14: **MSRC Schnupp 10 cm detuned** Power inside SRC for the 56 MHz sidebands (all modes).

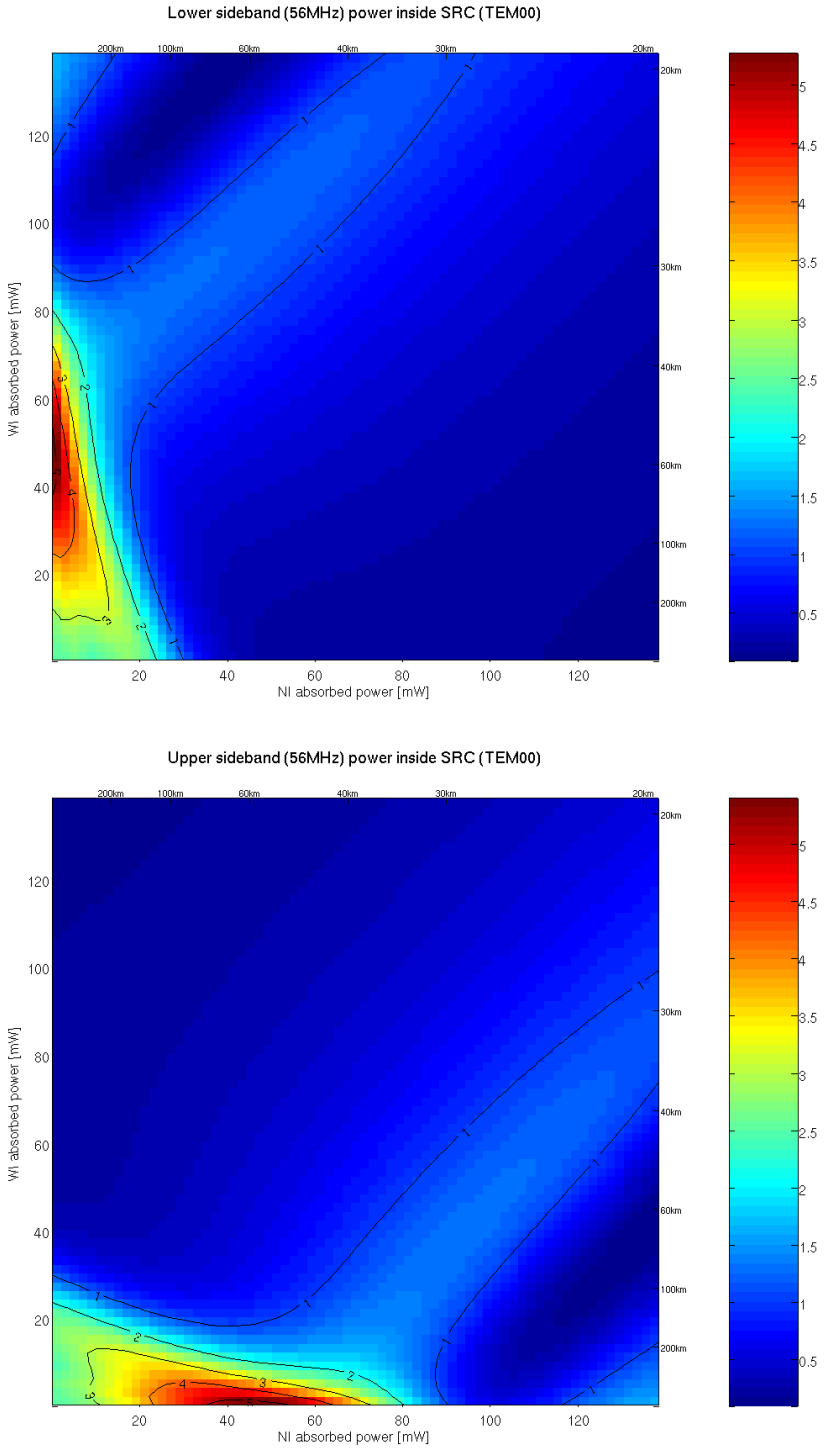

Figure 15: **MSRC Schnupp 10 cm detuned** Power inside SRC for the 56 MHz sidebands (only TEM_{00}).

3.4 Non-degenerate recycling cavities - Broad-band

Figures 16 and 17 show the 56 MHz sideband powers inside the PRC as a function of thermal effects. The behavior is quite different with respect to the marginally stable case. The only similarity is in the presence of two high recycling gain regions corresponding again to the differential lensings that introduce a dephasing such to cancel the Schnupp asymmetry. Since in the case of NDRC there is no significant loss of sideband powers due to degeneracy into high order modes, one would expect no large decrease of sideband powers as common lensing increases. The two plots show indeed an increase of sideband recycling gains inside PRC as common mode lensing increases. Even if puzzling at first sight, this can be easily understood. In NDRC as well as in MSRC the result of common mode lensing is a dephasing in the TEM_{00} sideband mode in reflection of the Michelson part. This additional dephasing is compensated inside PRC by the PRCL lock, while it is not inside SRC since the tuning is maintained at the nominal broad-band point. Therefore as common mode lensing increases, the signal recycling cavity is brought out of resonance for the 56 MHz sidebands and its reflectivity increases. This explains why the recycling gain inside PRC increases.

Figures 18 and 19 show the 56 MHz sideband powers inside SRC. These are almost complementary to the PRC powers and as expected there is no large common lensing effect. The change in sideband powers is not as large as one would naively expect moving the cavity out of resonance, but this is consistent with the change in coupling factor between the PRC and the SRC.

3.5 Non-degenerate recycling cavities - detuned

Figures 20 and 21 show the 56 MHz sideband powers inside PRC, while figures 22 shows the sideband powers inside SRC, for the 3 cm Schnupp asymmetry case. Similarly, figures 23, 24 and 25 refer to the 10 cm Schnupp asymmetry case. Sidebands are weakly sensitive to common mode lensing while there is a larger dependency on differential lensings.

3.6 Discussion

The behavior of second sidebands is as expected slightly more complex than the first ones, since they partially resonate inside SRC. However, provided a large enough Schnupp asymmetry is chosen to get good error signals for SRCL, the main conclusion is that there is no really new behavior of these sidebands with respect to the other one. In the MSRC case 56 and 6 MHz sidebands behaves qualitatively in the same manner, while in the NDRC case 56 MHz sidebands seem less critically sensitive to differential lensings than 6 MHz.

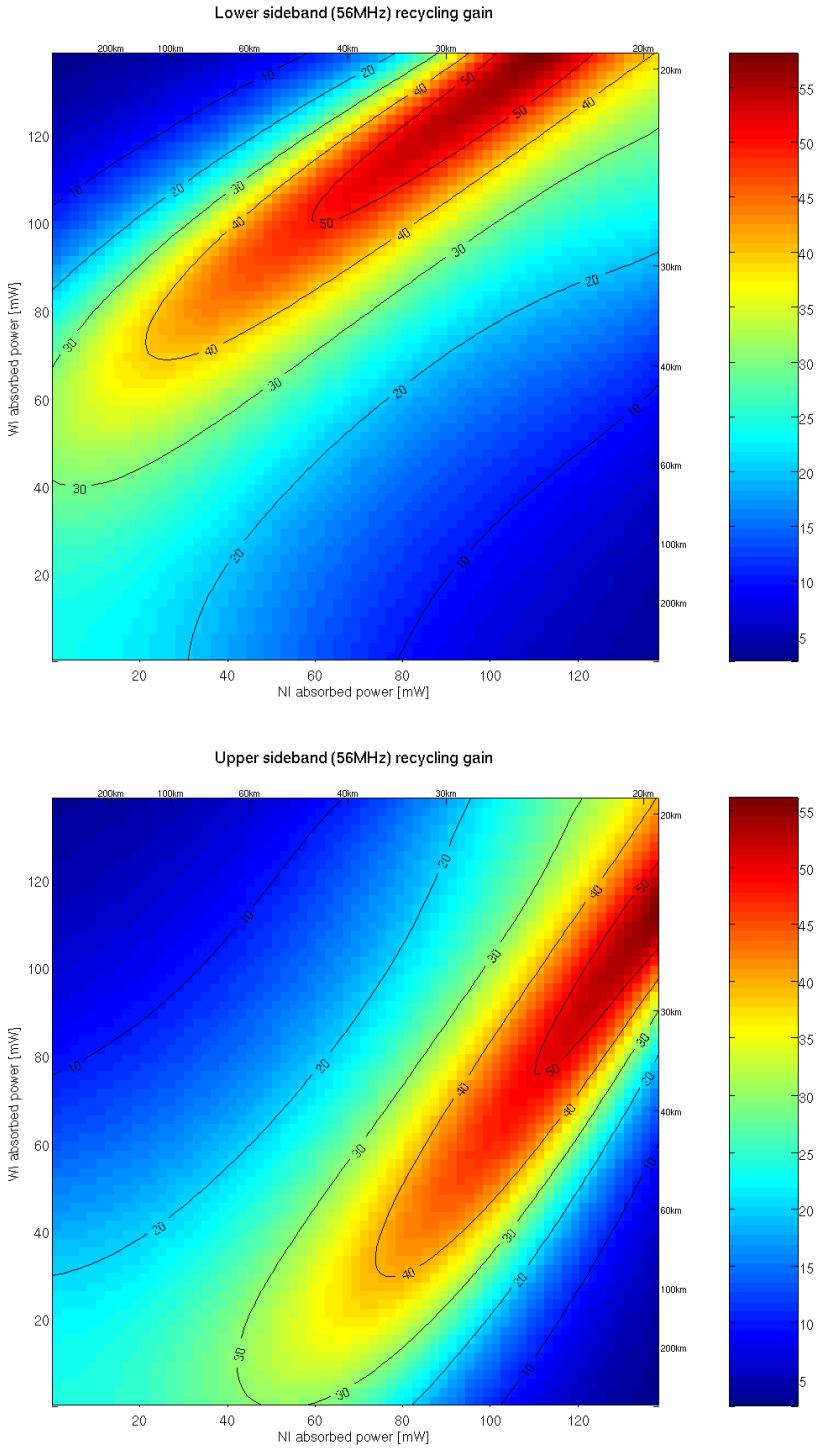

Figure 16: **NDRC Schnupp 3 cm broadband** Power inside PRC for the 56 MHz sidebands (all modes).

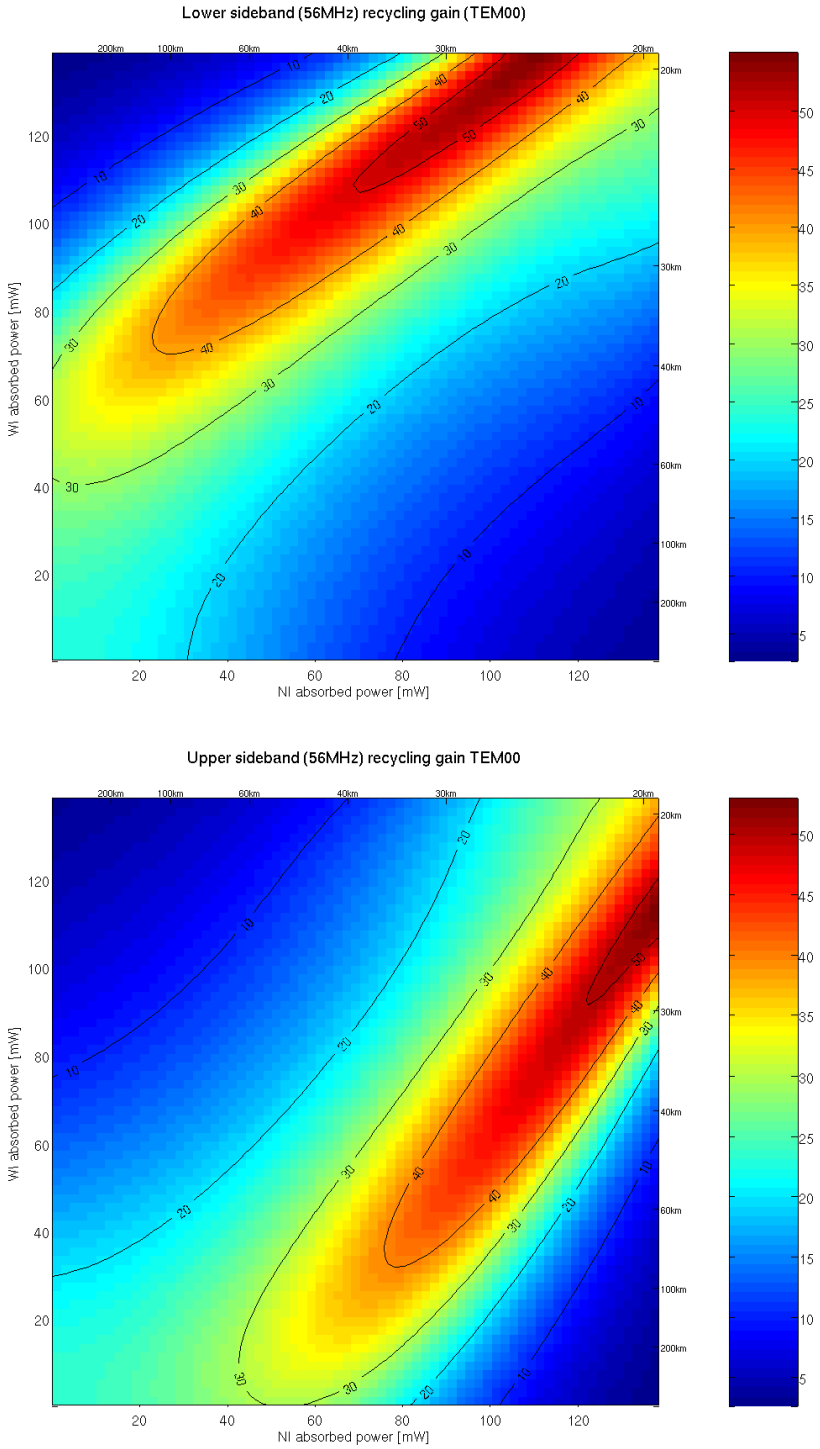

Figure 17: **NDRC Schnupp 3 cm broadband** Power inside PRC for the 56 MHz sidebands (only TEM_{00}).

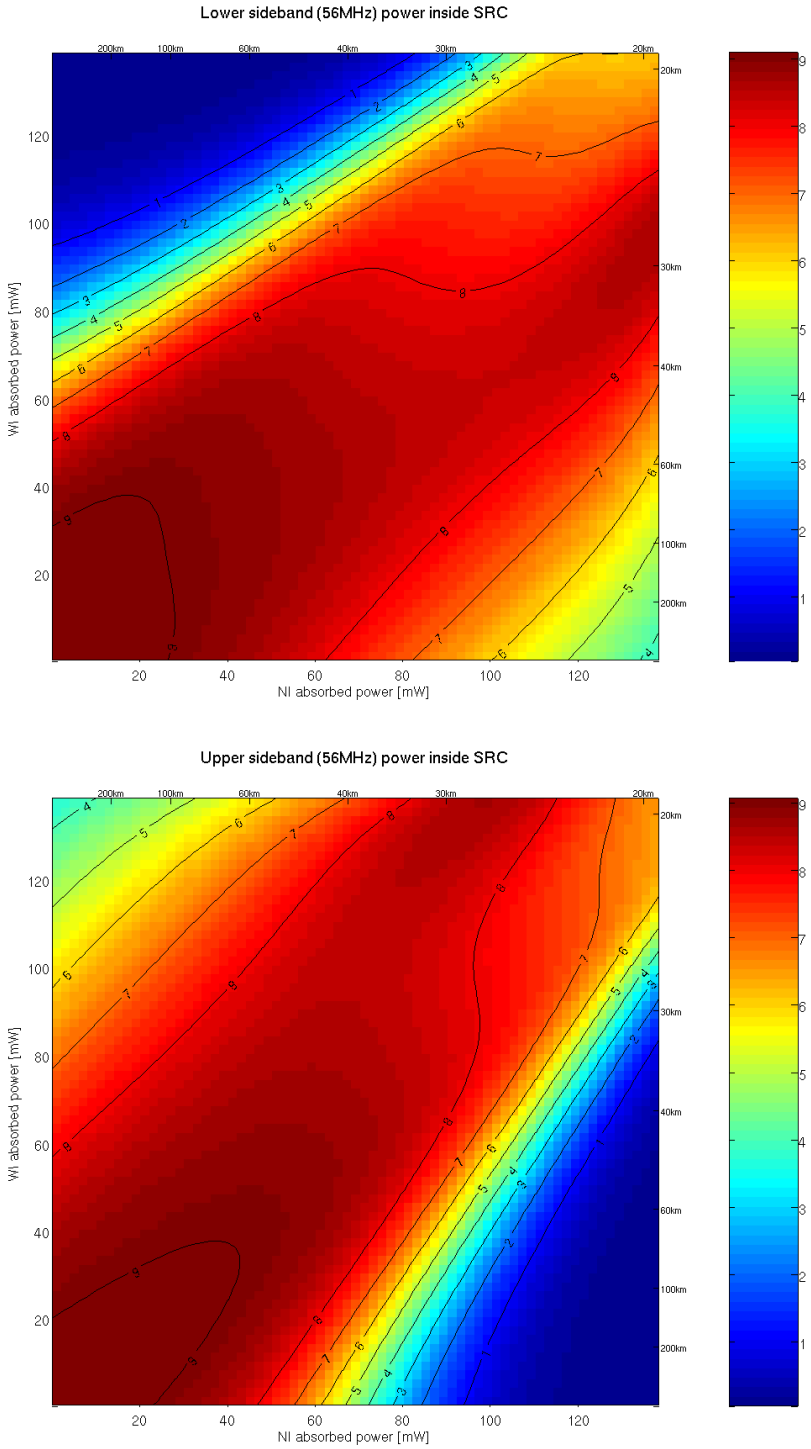

Figure 18: **NDRC Schnupp 3 cm broadband** Power inside SRC for the 56 MHz sidebands (all modes).

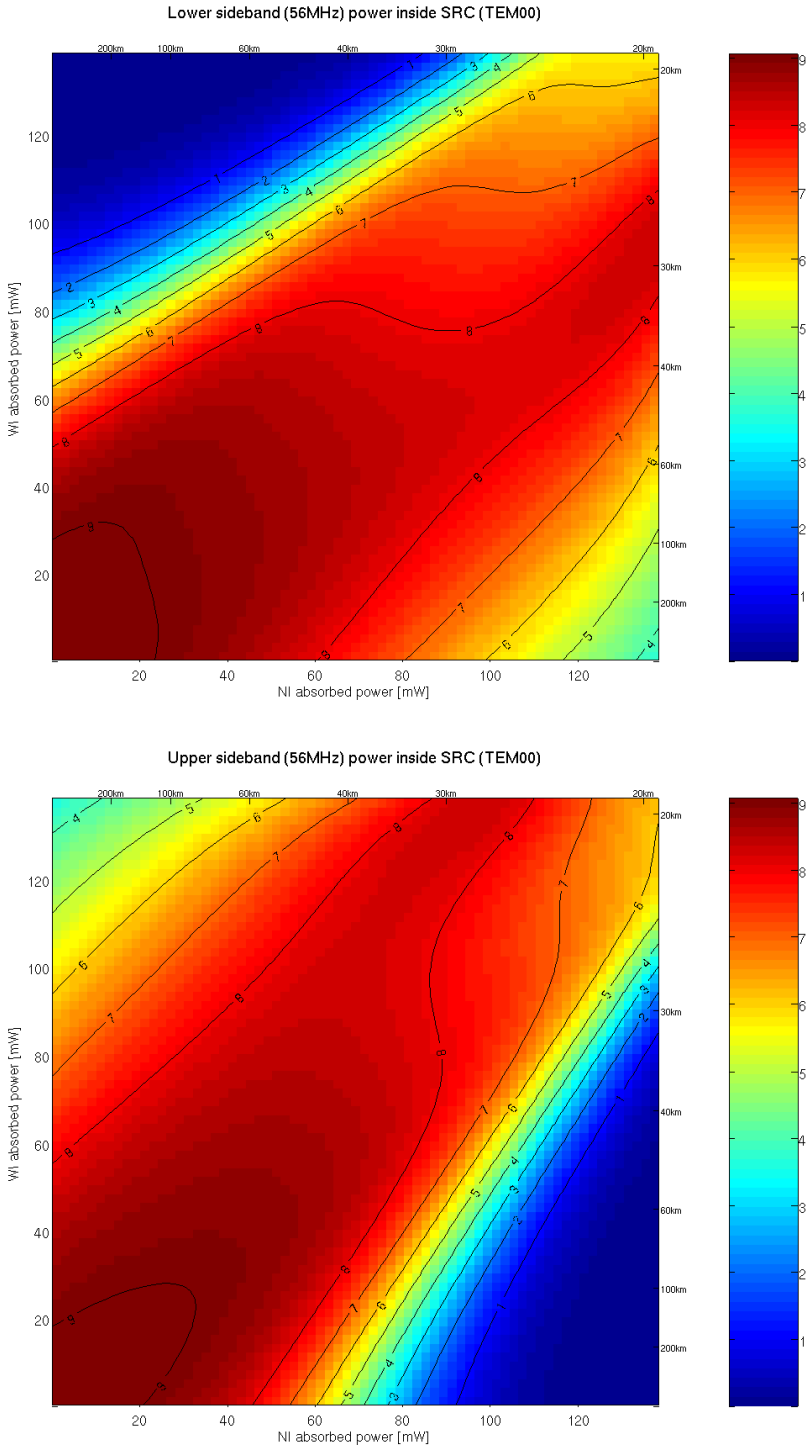

Figure 19: **NDRC Schnupp 3 cm broadband** Power inside SRC for the 56 MHz sidebands (only TEM_{00}).

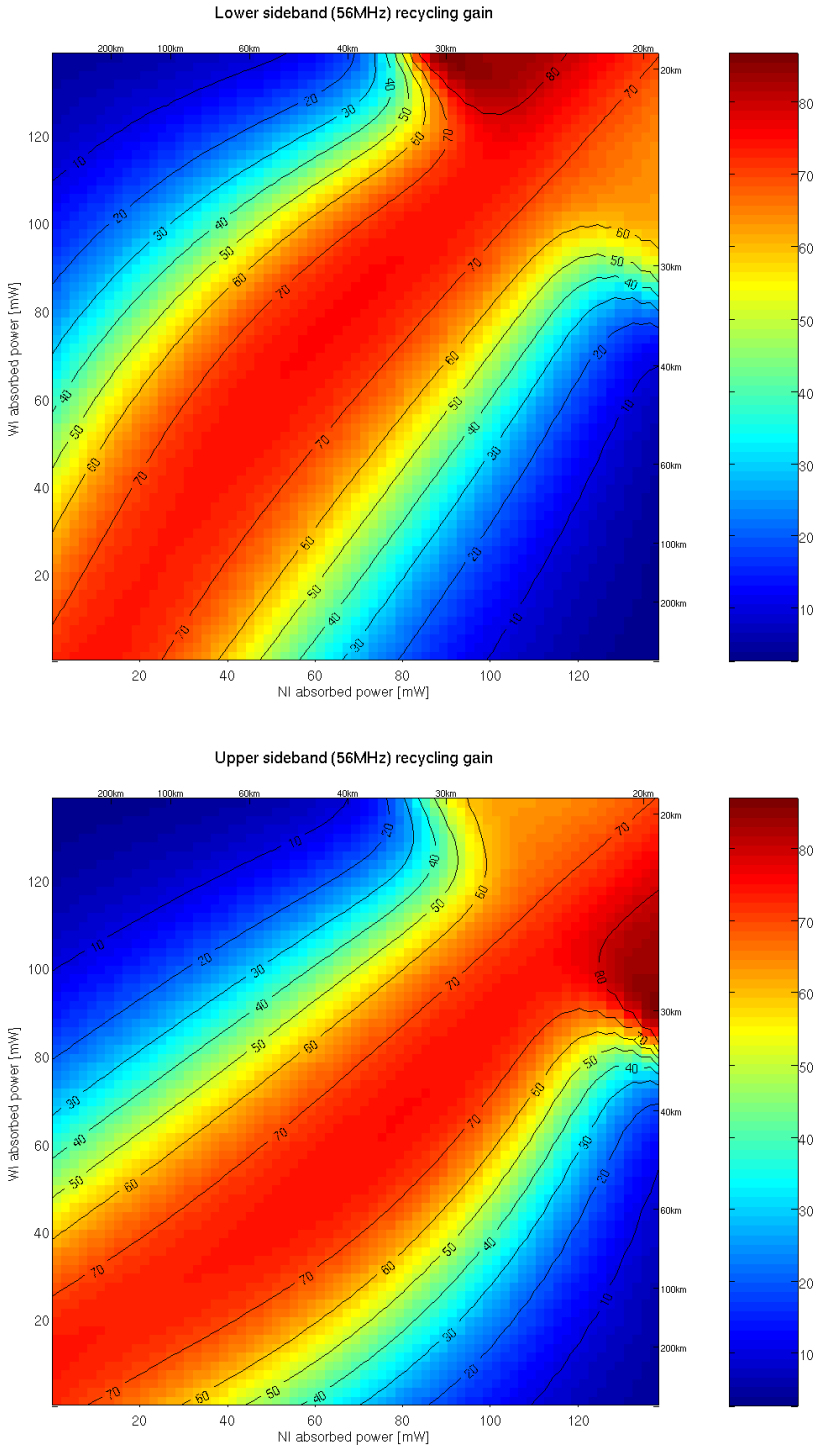

Figure 20: **NDRC Schnupp 3 cm detuned** Power inside PRC for the 56 MHz sidebands (all modes).

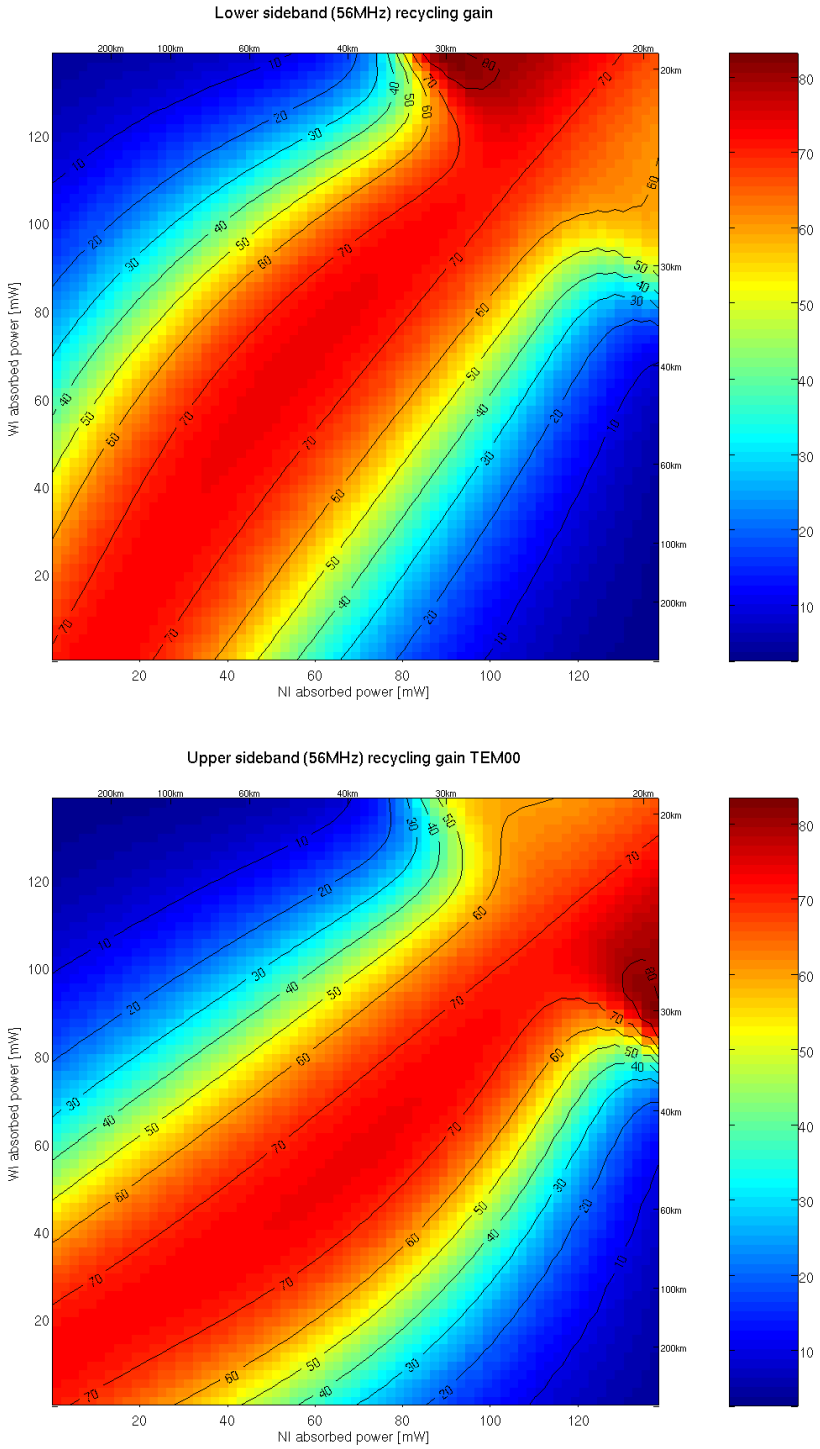

Figure 21: **NDRC Schnupp 3 cm detuned** Power inside PRC for the 56 MHz sidebands (only TEM_{00}).

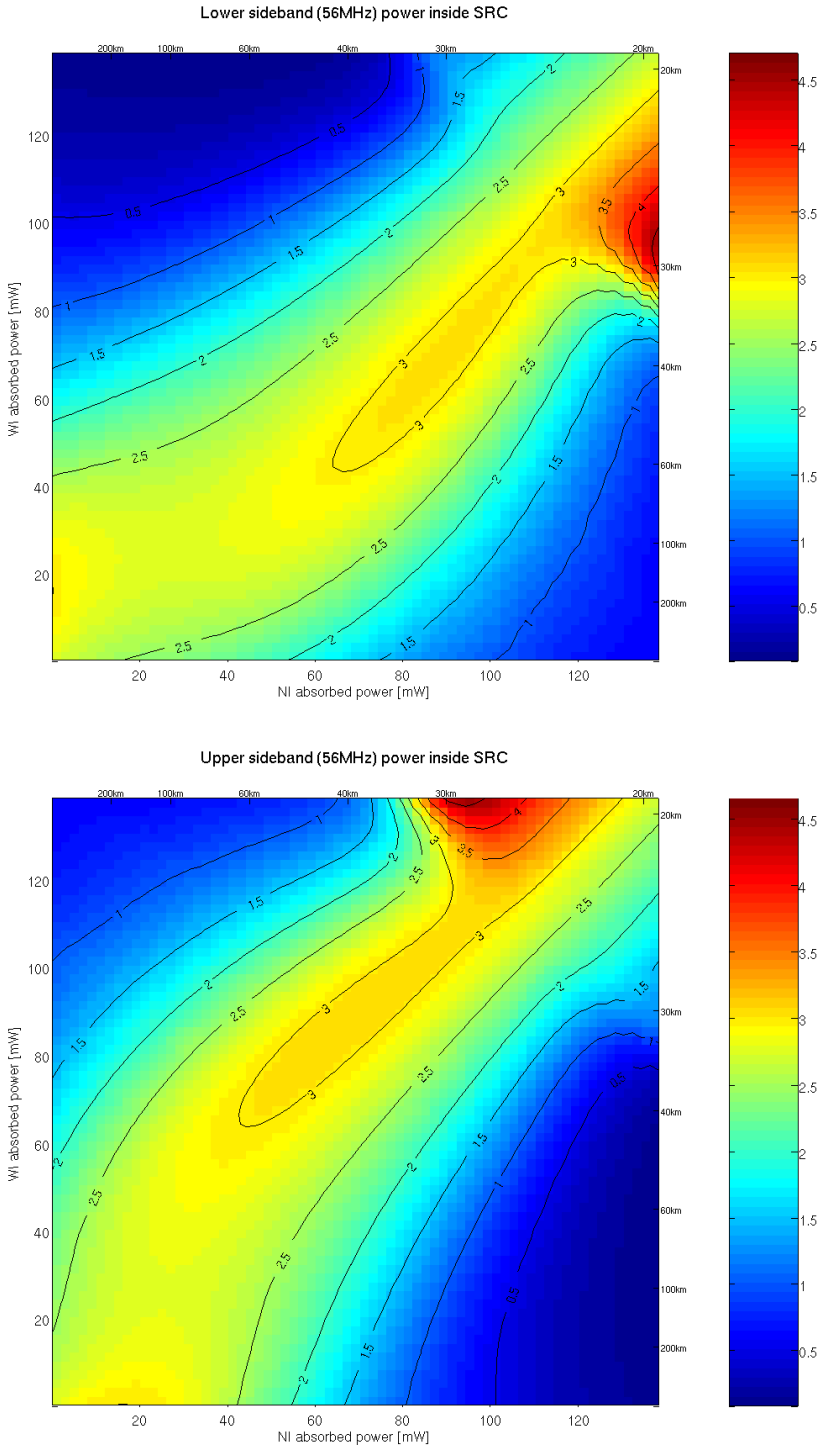

Figure 22: **NDRC Schnupp 3 cm detuned** Power inside SRC for the 56 MHz sidebands (all modes).

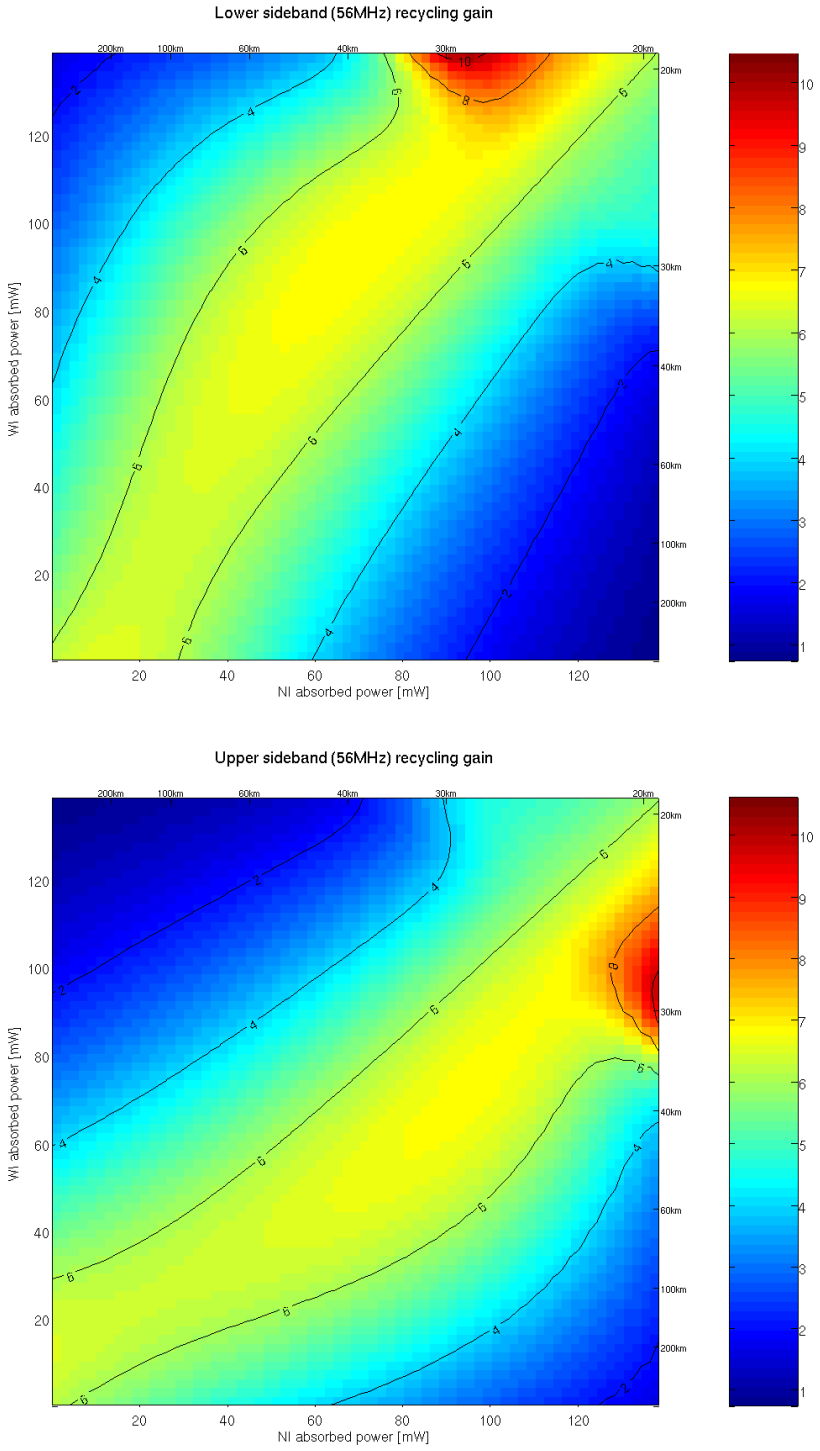

Figure 23: **NDRC Schnupp 10 cm detuned** Power inside PRC for the 56 MHz sidebands (all modes).

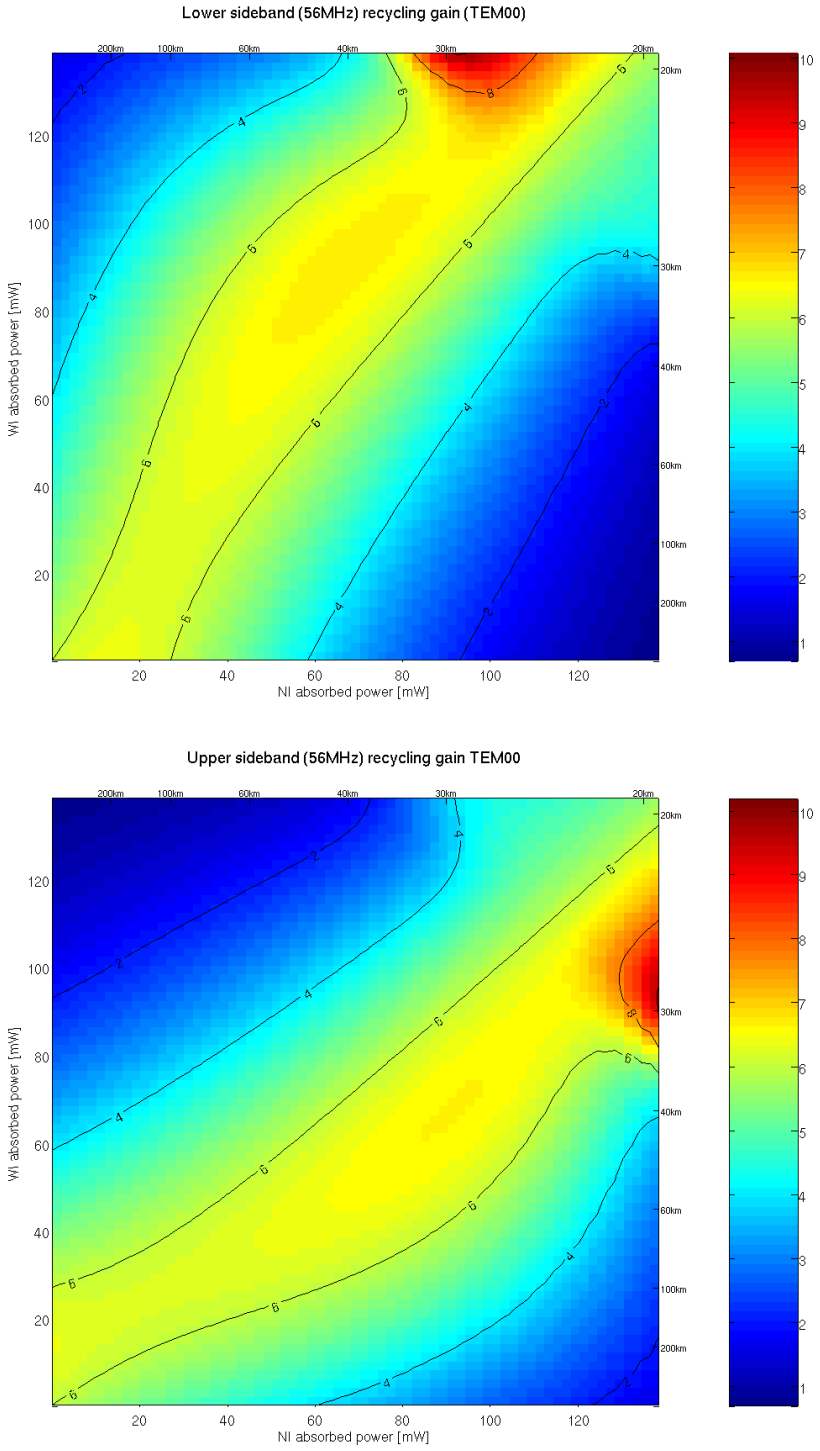

Figure 24: **NDRC Schnupp 10 cm detuned** Power inside PRC for the 56 MHz sidebands (only TEM_{00}).

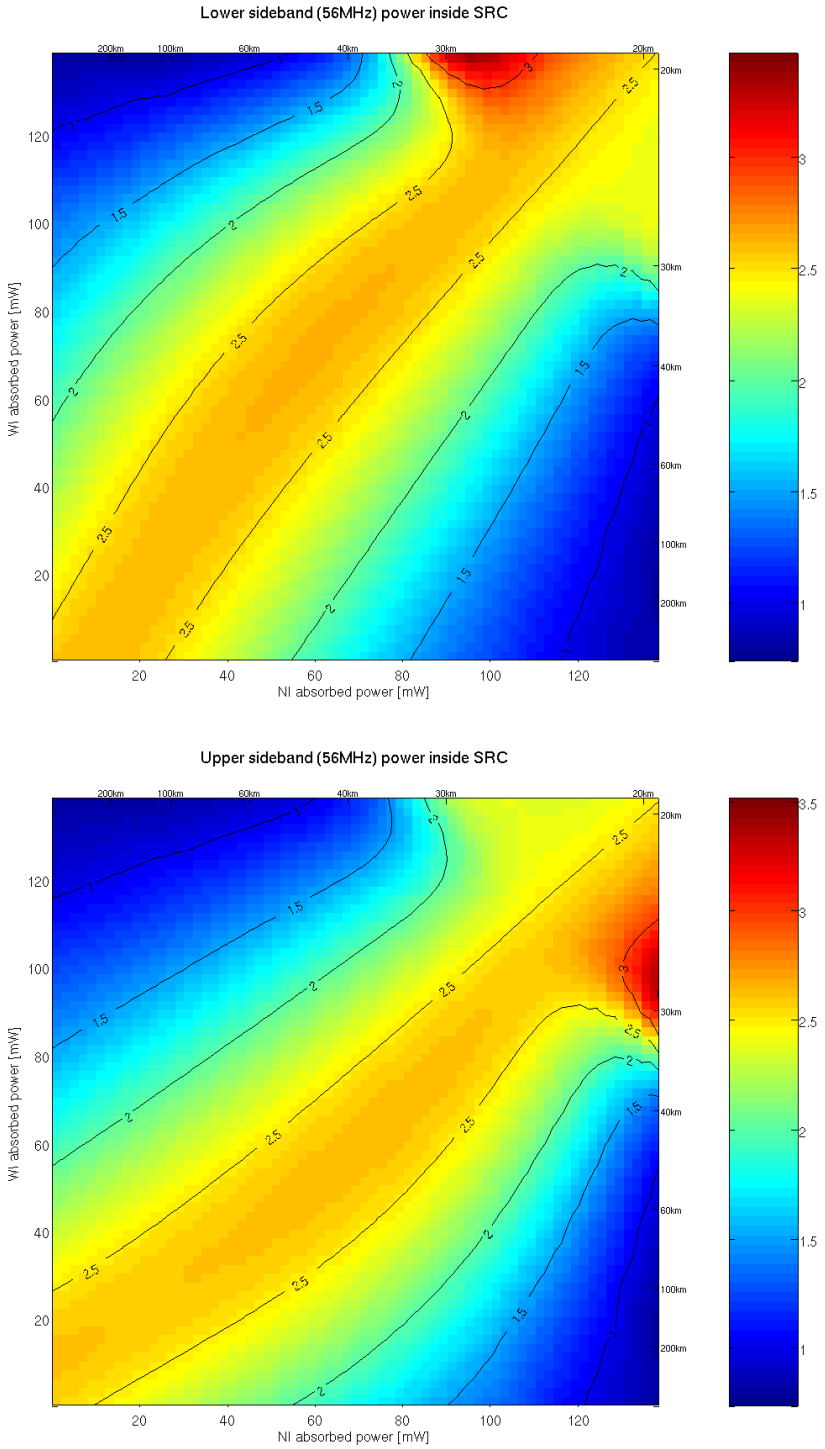

Figure 25: **NDRC Schnupp 10 cm detuned** Power inside SRC for the 56 MHz sidebands (all modes).

4 Finite size of mirrors

As already explained in [2], mirrors can be modeled with a finite size just limiting the numerical integration used to compute reflection operators to the correct size. In these simulations a coating diameter of 32 cm has been chosen, which correspond to 2.5 times the spot size at the end mirrors. This size has been used for arm cavity mirrors.

In the case of MSRC the power recycling mirror is a large mirror modeled with a 32 cm diameter coating as the arm cavity one. In the NDRC case the full telescope is simulated, but clipping is considered only at PRM3 and SRM3 level, since these are the largest mirrors where the beam is also large. The other mirrors are supposed to be smaller, but the spot size on them is also very small. PRM3 and SRM3 are assumed to have a coating of 32 cm in diameter.

The simulations shows that the only relevant effect of introducing a finite mirror size is a loss in sensitivity also without thermal effects (see fig. 26). This is understandable since clipping is increasing the total round trip losses inside arm cavities.

The behavior in presence of thermal effects is not significantly different from what is obtained with ideal infinite mirrors.

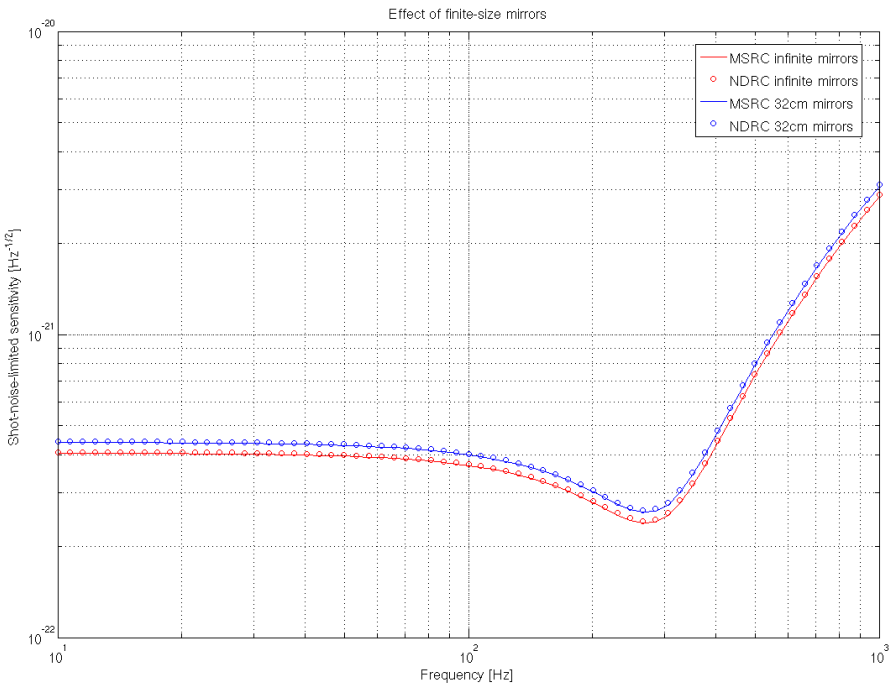

Figure 26: Effect on sensitivity of the finite size of mirror coatings, without thermal effects.

5 Behavior of error signal against thermal effects

Once all carrier and sideband fields are computed, it is possible to reconstruct the demodulated error signals that can be used for the ITF control. Fields at three main points are used:

- the field inside PRC is taken in reflection of PR mirror inside the cavity. The information contained in this beam is the same as any pick-off at the beam splitter or input mirror level;

- the field reflected by the ITF;
- the dark fringe field, which is equivalent to the field inside SRC except for the signal recycling mirror transmission.

All these signals can be demodulated at the two modulation frequencies. These signals have been studied with a perfect ITF, without thermal effects, to select the most suitable ones to control each degree of freedom. The selected signals are:

D.O.F.	**Signal**
DARM	dark fringe DC TEM_{00} power (`DF_DC`)
CARM	PRC demodulated in phase at 6 MHz (`PRC_P1`)
PRCL	ITF reflection in phase at 6 MHz (`REF_P1`)
SRCL	PRC demodulated in phase at 56 MHz (`PRC_P2`)
MICH	PRC demodulated in quadrature at 56 MHz (`PRC_Q2`)

Once error signals are computed one can use them to lock the interferometer, or in other words to implement a different technique to optimize the working point with respect to the pseudo-control explained in [1]. The error signals are used as inputs for simple feedback loops that act changing the static tuning of all degrees of freedom. The loops are implemented using simple integrators: while this control is theoretically unconditionally stable, it is in practice limited by the linear range of the error signals. However, once proper gains have been set up looking at the Pound-Drever-Hall signal slopes without thermal effects, the locking loops converge typically in less than 100 iterations. The convergence criteria is set by the error signals to become simultaneously smaller than a given threshold, independently tuned for each degree of freedom.

Since the behavior of SRCL error signal is not yet well understood in both MSRC and NDRC cases, this control loop is left open and the position found with the pseudo-control is used for the SRC tuning [1]. All other loops are closed, including MICH which was not optimized in the previous simulations.

A direct comparison of the results of the two locking algorithm is presented in figures 27, 28, 29, 30, 31 and 32 for the NDRC case. Corrections are slightly different in the two cases, mainly in the differential lensing direction, but the behavior of all fields is comparable. In particular the loss of 6 MHz sideband powers with differential thermal effects is still present (fig. 28), even if the MICH lock changes it a bit. The behavior of 56 MHz sidebands (fig. 29) is better balanced as an effect of MICH locking loop using a PRC signal.

This lock algorithm works also in the case of MSRC, but results are not presented here since they add no significant information to the discussion.

6 Conclusions

The destructive effect of differential defects on 6 MHz sideband recycling gain has been confirmed to hold also for small mis-alignments. It seems even more probable that differential mis-alignment and residual lensings will pose serious problems for lock acquisition.

The real finite size of mirrors have been simulated, showing that in presence of clipping on arm cavity mirrors or in PRM3 or SRM3 there is no significant difference in the interferometer behavior with respect to thermal effects. Clipping at the level of the other recycling mirrors have not been considered.

The behavior of second sidebands (56 MHz in this simulations) has been simulated and understood. These sidebands behave in a more complex way with respect to 6 MHz ones, but they do not introduce additional constraints neither for MSRC or NDRC. One important point is that in order to extract suitable error signals to control SRCL the Schnupp asymmetry must be increased to about 10 cm.

Finally real error signals have been simulated and used to lock the interferometer. Results are comparable to what obtained with the already established pseudo-control strategy [1]. The additional feature is the lock of the MICH degree of freedom. Since the signal used to lock it comes from the 56 MHz sidebands, their behavior is improved. The sensitivity of 6 MHz sidebands to differential effects is slightly changed but not canceled.

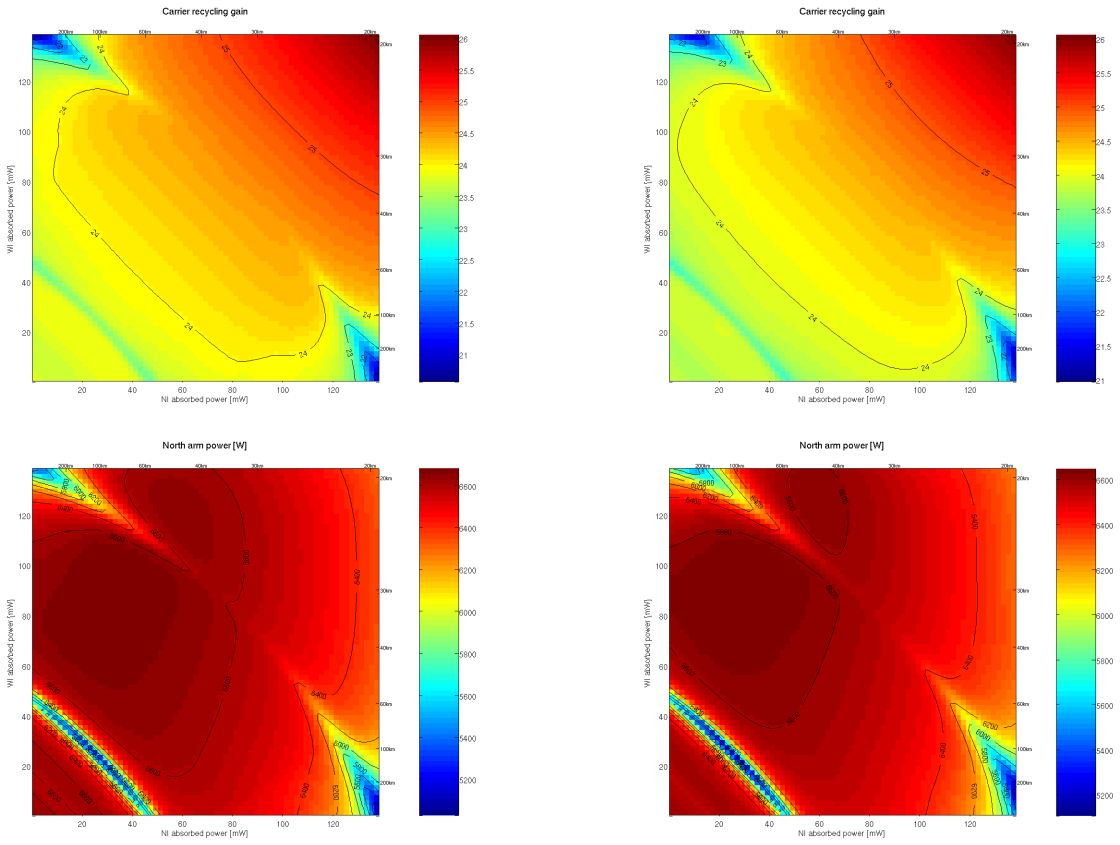

Figure 27: Carrier recycling gain (top) and power inside north arm (bottom) for astigmatic NDRC, comparing the result of the new locking algorithm (right) with the old pseudo-lock algorithm (left).

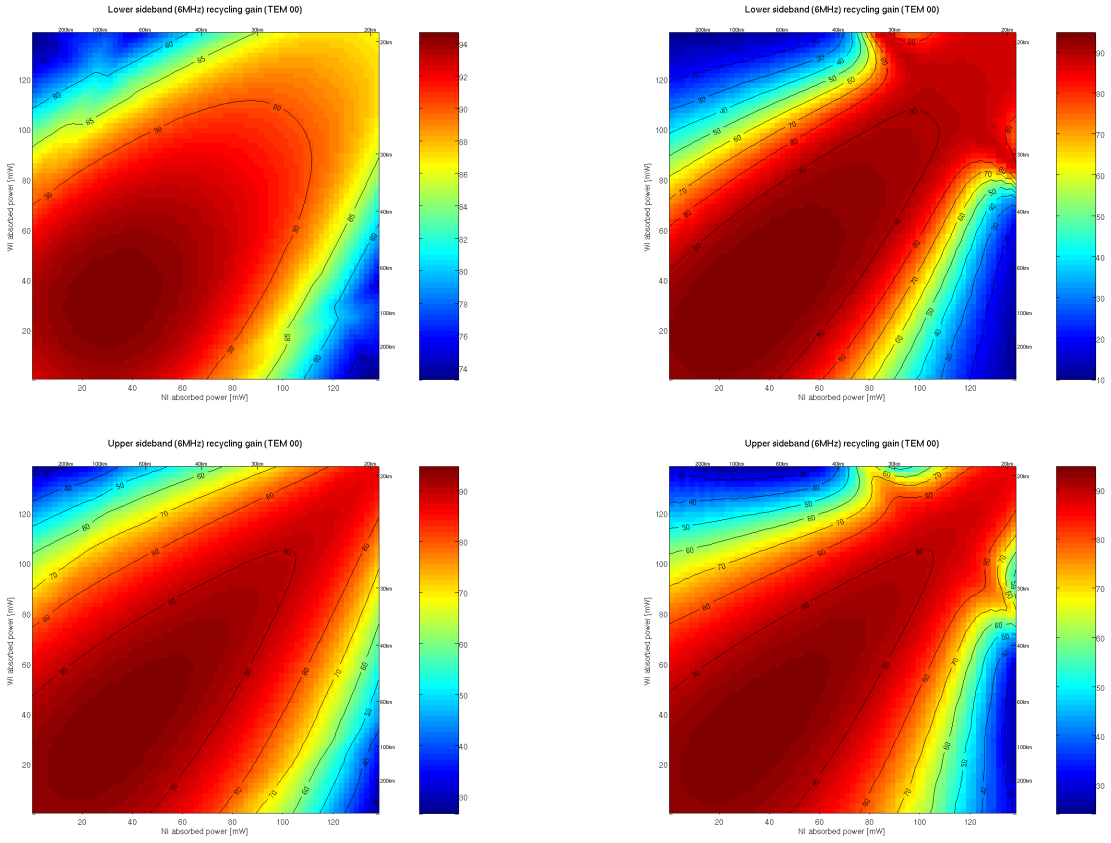

Figure 28: Lower (top) and upper 6 MHz sideband (bottom) behavior for astigmatic NDRC, comparing the result of the new locking algorithm (right) with the old pseudo-lock algorithm (left).

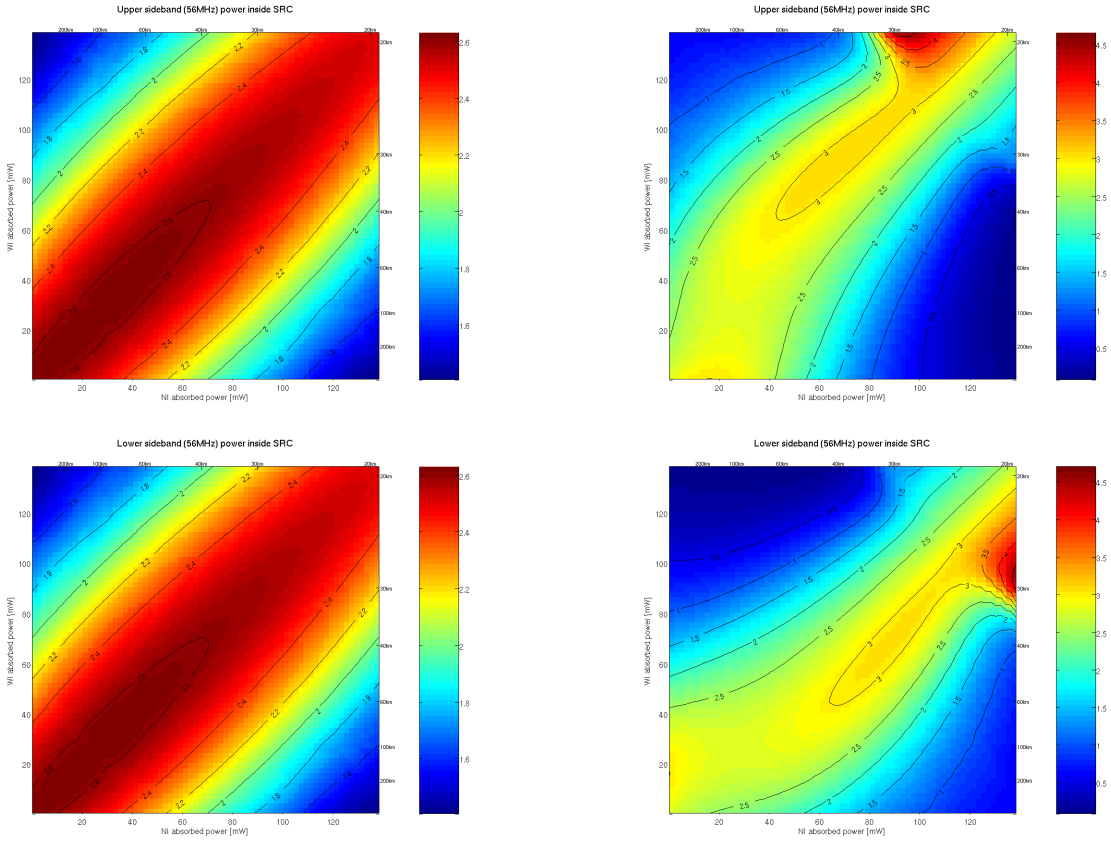

Figure 29: Upper (top) and lower (bottom) 56 MHz sideband power inside SRC for astigmatic NDRC, comparing the result of the new locking algorithm (right) with the old pseudo-lock algorithm (left).

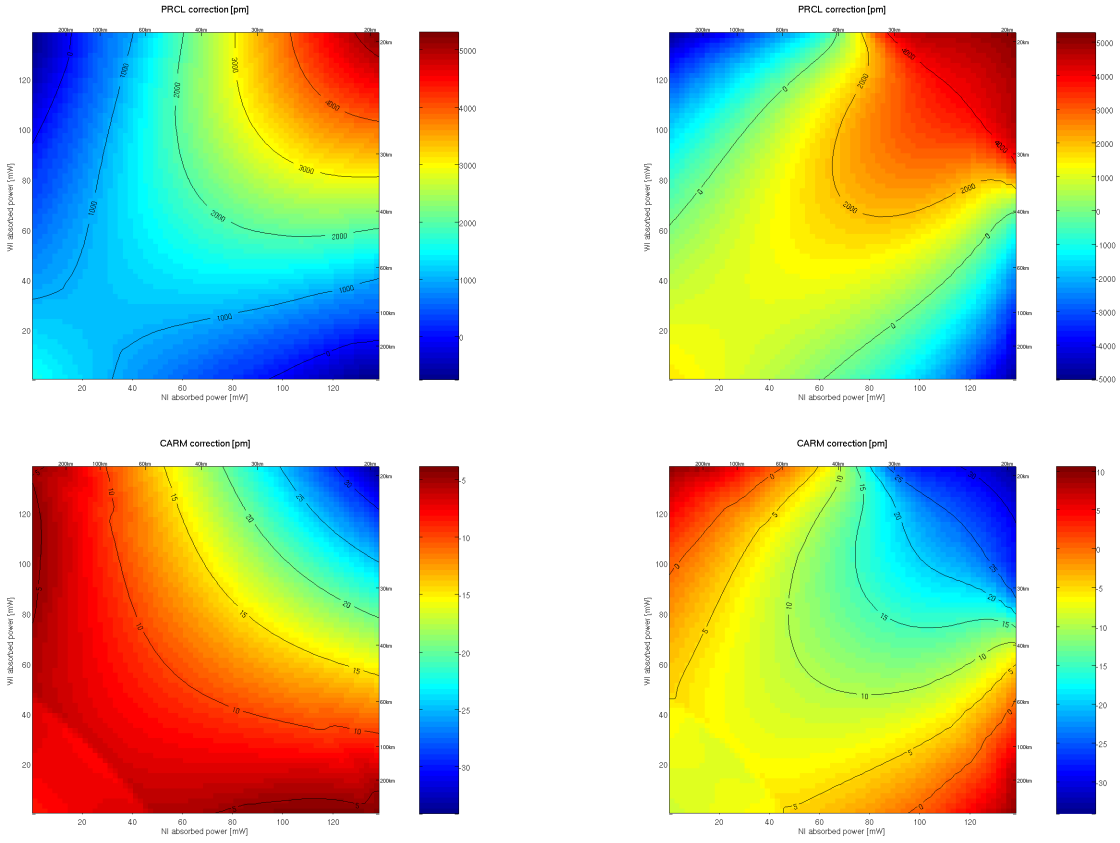

Figure 30: PRCL (top) and CARM (bottom) correction signals for astigmatic NDRC, comparing the result of the new locking algorithm (right) with the old pseudo-lock algorithm (left).

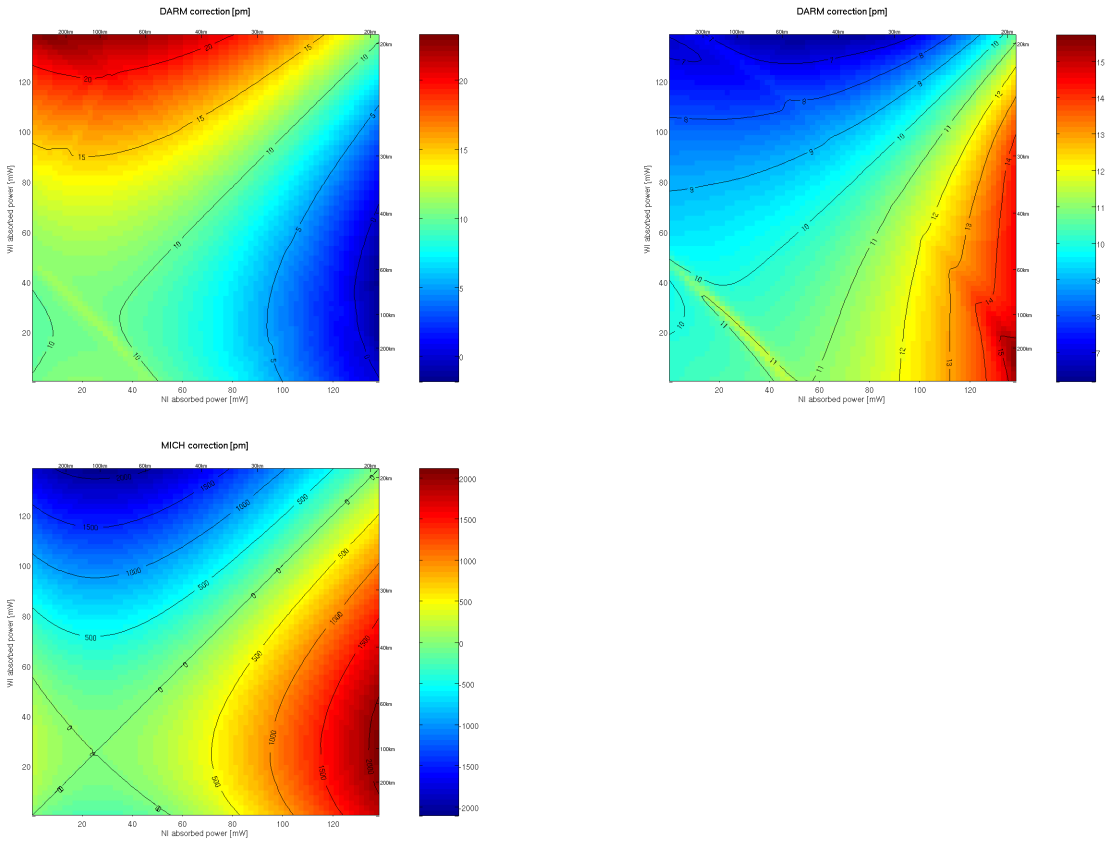

Figure 31: DARM (top) and MICH (bottom) correction signals for astigmatic NDRC, comparing the result of the new locking algorithm (right) with the old pseudo-lock algorithm (left).

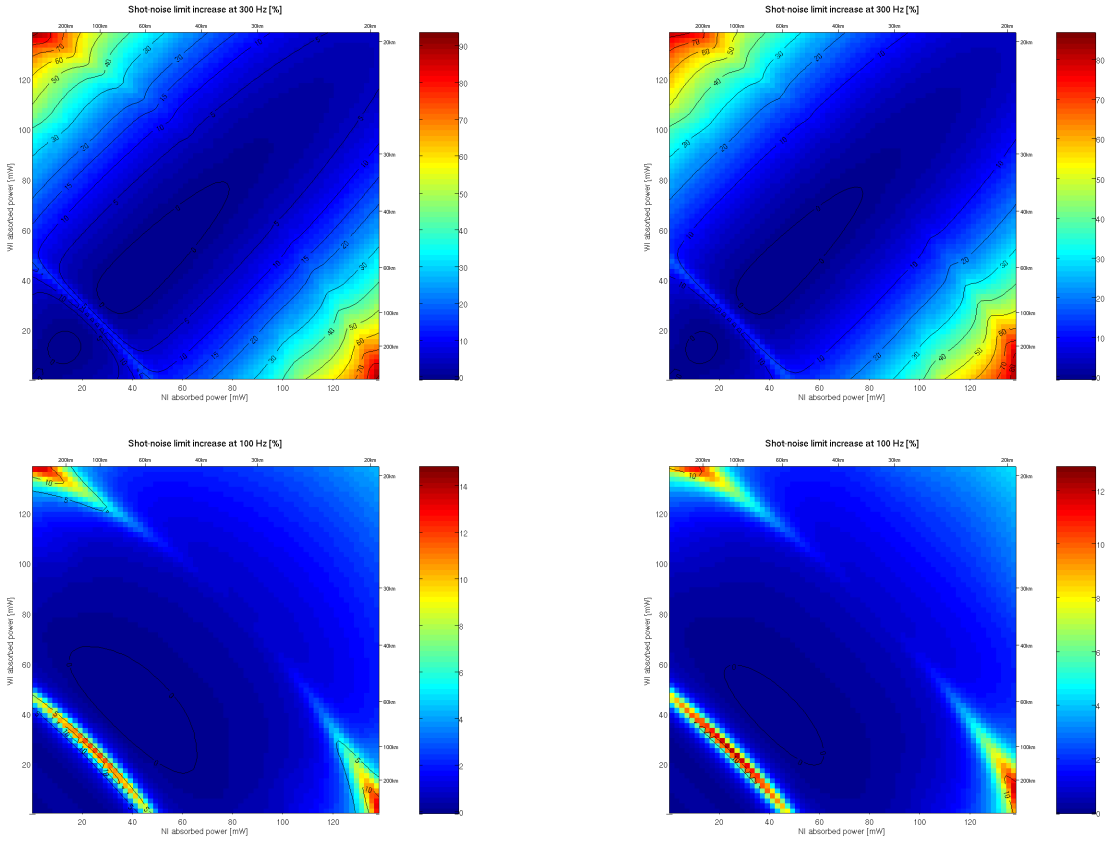

Figure 32: Sensitivity loss at 300 Hz (top) and 100 Hz (bottom) for astigmatic NDRC, comparing the result of the new locking algorithm (right) with the old pseudo-lock algorithm (left).

References

[1] G. Vajente, J. Marque, *Simulations of Advanced Virgo recycling cavities and thermal effects*, VIR-0148A-10 (2010) 1, 3, 29

[2] G. Vajente, *Modal Interferometer Simulation*, VIR-0142A-10 (2010) 28

[3] The Virgo Collaboration, *Advanced Virgo Baseline Design*, VIR-027A-09 (2009) 1